

Article

CCTV Camera Array for the Displacement and Strain Measurement of a Beam Specimen in a Laboratory

Rujika Tuladhar ¹, Punchet Thammarak ¹ and Said Elias ^{2,*} 

¹ Structural Engineering, Asian Institute of Technology, School of Engineering and Technology, Pathumthani 12120, Thailand

² Department of Construction Management and Engineering (CME), Faculty of Engineering Technology (ET), University of Twente (UTWENTE), 7522 Enschede, The Netherlands

* Correspondence: elias.rahimi@utwente.nl

Abstract: The available conventional sensors, like displacement transducers, used in the Structural Engineering Laboratory are expensive. In addition to that, the need for data acquisition devices also escalates the expense invested in point contact measurement systems. The recent appeal of vision-based measurement and the search for cost-effectiveness has led to an exploration of the established sampling moiré method using cheap closed-circuit television (CCTV) cameras as a viable option. The sampling moiré method is simple and analyzes the displacements from grating images by a phase-shifting method. Several trial experiments were conducted, which demonstrated that the setup is at least as accurate as the traditional measuring system. An experiment was conducted on a steel I-beam for displacement measurement, which displayed satisfactory results. In addition, the setup was also tested for strain measurement, and it has yielded promising results that need fine-tuning. This paper discusses the challenges, findings, and the possibility of incorporating vision-based displacement measurements in laboratory platforms.



Citation: Tuladhar, R.; Thammarak, P.; Elias, S. CCTV Camera Array for the Displacement and Strain Measurement of a Beam Specimen in a Laboratory. *Buildings* **2022**, *12*, 1778. <https://doi.org/10.3390/buildings12111778>

Academic Editors: Shibin Lin, Donghui Yang, Sadegh Shams and Chunxu Qu

Received: 13 September 2022

Accepted: 20 October 2022

Published: 24 October 2022

Publisher's Note: MDPI stays neutral with regard to jurisdictional claims in published maps and institutional affiliations.



Copyright: © 2022 by the authors. Licensee MDPI, Basel, Switzerland. This article is an open access article distributed under the terms and conditions of the Creative Commons Attribution (CC BY) license (<https://creativecommons.org/licenses/by/4.0/>).

Keywords: vision-based measurement; sampling moiré method; CCTV camera; image processing; displacement and strain

1. Introduction

The virtue of remote access and non-contact-based optical techniques are gaining popularity for deformation measurement. Traditional deformation measurement technologies such as Linear Variable Differential Transformers (LVDTs), strain gauges, etc., necessarily require physical access to a structure and are suitable for point measurements only. This interference has led to vision-based methods garnering great research interest in recent times [1]. Non-contact computer-vision-based monitoring techniques using cameras are gaining popularity in the sector of structural health monitoring (SHM) as efficient and effective sensing techniques.

The measurement of the displacement and distribution of strain has been the main concern for monitoring the integrity and safety of structures. They have been significant for the purpose of design validation, performance monitoring, and safety assessment. The available options to obtain displacement and strain distribution is by using sensors and strain gauges at various locations, which can ensure only measurement at one location. Apart from this, setting up these sensors requires considerable time and it is expensive, as well, to obtain a representative idea of the condition of a structure [2].

In order to overcome this condition, full-field noncontact optical methods have been used, such as the digital image correlation method, moiré interferometry, speckle interferometry, phase-shifting digital holography, the moiré grid method, holographic interferometry, shearography, etc. These methods are fairly effective to attain high spatial resolution within a short time interval in comparison to the point measurement technique. Particularly, the

moiré method has been in practice as a measurement tool of displacement and strain as a vision-based method for whole-field information [3].

The sampling moiré method is a novel moiré method that uses a phase analysis technique through the image processing of the grating pattern to measure displacement, strain distribution, and shape. This method uses a charge-coupled device (CCD) or complementary metal-oxide semiconductor (CMOS) sensor to capture a single image of a specimen grating of known pitch during deformation. Only one image is handled to evaluate the phase distribution by generating multiple phase-shifted moiré patterns by the thinning-out, down-sampling, and interpolation of the sequential pixels through phase analysis [2–15]. Through the phase difference of the moiré fringe prior to deformation to that of post-deformation, the displacement distribution is attained.

Studies are available on the sampling moiré method ranging from those on performance and accuracy checking to applications in real-world cases. They have highlighted the fact that the method is a simple and easy procedure with high accuracy and analysis speed in addition to low-cost performance. Computer simulations were carried out to authorize the effectiveness of this method through a phase compensation methodology [5,6] to reduce the large phase error that exists when the sampling pitch does not match the grating pitch. Similarly, simulations were also performed to establish the accuracy of the method, concluding that cosinusoidal grating performed best while rectangular grating can perform just as well with camera defocusing [3,7]. Moreover, there have been experiments performed to confirm the effectiveness of the method through a three-point bending test conducted on a symmetrical rectangular steel beam for deflection measurement [2–4,16–18]. The results of the experiment display that the displacement values calculated by using the method comply with that of the displacement sensor and theory and ensure the accuracy of the method. In addition to that, there are studies that have determined the shape and displacement of the object along with strain determination at the same position points before and after deformation [19] and an experiment conducted to determine the three-dimensional (3-D) shape and strain distribution of a rotating tire [9,20]. Both of these were conducted using two cameras to capture the images and even the shape determination of a trapezoidal object by pasting the grating on the top of the object [20]. Moreover, the experiment conducted on grating over a rubber belt stretched in orthogonal directions for strain measurement revealed that the method was suitable for the calculation of large, deformed objects with little deviations from the theoretical strains [2,19,20]. Likewise, in terms of applications in the field of civil engineering, the method was able to detect submillimeter deflection effectively in an experiment conducted on a ceiling-traveling crane [7]. Another application was conducted on a fixed concrete bridge to conduct dynamic deformation measurements by the movement of a train in real-time [21]. Moreover, this has been expanded to the displacement measurement of a concrete bridge for a high-speed railway in Japan using retroreflective moiré markers. The two-dimensional (2-D) in-plane displacements at multiple locations could be easily measured from recorded digital images [11], even for the measurement of the deflection and vibration of a large-scale concrete bridge from captured video with a commercial cinema camera [12] in recent times. Further, in terms of experiments, comparative experiments conducted in a columnar cantilever beam connected to a loading jack and laser displacement meter demonstrated the effectiveness of the method for deformation measurement when the errors between the measurements were compared [14,21]. Different cameras were used for the damage detection of bridges under different loading conditions [22–29].

A sampling moiré camera is a compact system with a CMOS sensor, memory unit, and processing unit that analyzes the grating images and provides output in real-time. The laboratory part of the experiment for close-range displacement conducted in a small displacement detection system to measure landslide [8] forms the basis for this study. The use of a translation guide to assure the accuracy of the displacement measurement has been carried out, similar to the study that uses an electronic motion stage. This study focuses on addressing the implementation and augmenting the usability of the principle of the

moiré method at a laboratory scale using closed-circuit television (CCTV) cameras. Several laboratory trials were conducted to characterize the influence of factors such as the target distance from the camera and optimal grating size on measurement performance. This was established by verifying the performance of the sampling moiré method using the CMOS sensor Mars series and then using the scheme with CCTV cameras, a platform for trials to later be deployed to specimen testing.

The applicability of the principle of the sampling moiré method to the laboratory platform has been explored here. The implementation of this scheme could open new doors to supersede the functionality of traditional techniques that are otherwise expensive. For example, the cost of the displacement transducer alone is 50 K Baht, excluding the cost of the data logger. Even if 12 units of CCTV cameras, each costing around 2 K Baht (52.40 US Dollars), were used, the overall setup would cost us around 35 K Baht (917.08 US Dollars). This experiment seeks to make use of a vision-based measurement technique and find displacement and strain simultaneously for deployment in a laboratory environment.

2. Methodology

2.1. Principle of Sampling Moiré Method

This sampling moiré method is an efficient phase analysis technique that performs an analysis of phase distribution on a single shot image. The fundamental principle is illustrated in Figure 1. In this method, fringes are gained by “down-sampling” from sequential pixels followed by “intensity interpolation”. By phase shifting spatially, i.e., changing the start-sampling pixel point in succession such that the sampling interval is similar to the pitch of the specimen grating, a series of moiré patterns can be attained. Eventually, from the series of phase-shifted moiré patterns, the phase of the moiré fringe is analyzed by using the phase-shifting method [2,3,13–15].

In Figure 1h–k, the k -th phase-shifted images can be shown approximately as follows:

$$I_k(i, j) = I_a(i, j) \cos \left[\phi_m(i, j) + 2\pi \frac{k}{N} \right] + I_b(i, j) \quad (k = 0, 1, 2, \dots, N - 1) \quad (1)$$

where $I_b(i, j)$ represents background intensity in the image, $I_a(i, j)$ represents the amplitude of the grating intensity, and $\phi_m(i, j)$ is the initial phase value of the moiré fringe.

The phase distribution of the moiré pattern can be obtained from frequency 1 of a discrete Fourier transform (DFT) algorithm or phase-shifting method using the Fourier transformation (PSM/FT) of Equation (1). Now, the value of the wrapped phase ϕ for frequency 1 is represented in the equation below.

$$\phi_m(i, j) = -\tan^{-1} \frac{\sum_0^{N-1} I_k(i, j) \sin(k \frac{2\pi}{N})}{\sum_0^{N-1} I_k(i, j) \cos(k \frac{2\pi}{N})} \quad (2)$$

The phase obtained by Equation (2) is wrapped by 2π and lies between $-\pi$ and π , which creates discontinuous deformation while calculating. Thus, a phase unwrapping algorithm must be combined by a local phase unwrapping algorithm to ensure accuracy in the measurement of strain distribution [22].

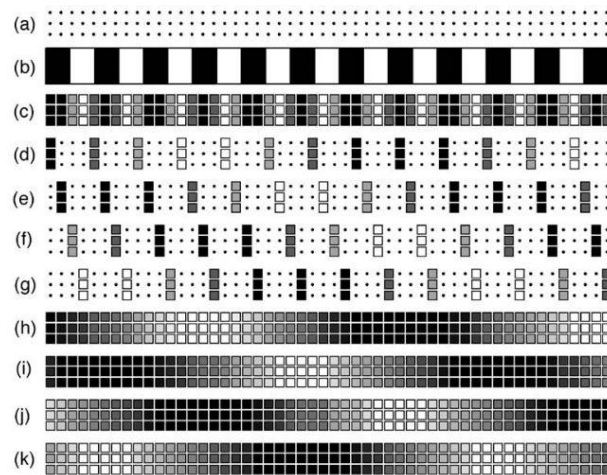


Figure 1. Phase analysis by sampling moiré method: (a) Sampling points of the camera; (b) specimen grating; (c) sampled image of (b); (d) thinned-out image from (c) ($N = 4$, $\alpha = 0$); (e) thinned-out image from (c) ($N = 4$, $\alpha = \pi/2$); (f) thinned-out image from (c) ($N = 4$, $\alpha = \pi$); (g) thinned-out image from (c) ($N = 4$, $\alpha = 3\pi/2$); (h) interpolated image of (d); (i) interpolated image of (e); (j) interpolated image of (f); (k) interpolated image of (g) (Adapted from [6]).

Phase ϕ_m of the moiré fringe is the subtraction of phase ϕ_r of the reference grating from phase ϕ_s of the specimen grating, such that:

$$\phi_m(i, j) = \phi_s(i, j) - \phi_r(i, j) \quad (3)$$

Phase ϕ_m of the moiré fringe has to be analyzed while phase ϕ_r of the reference grating remains unchanged. Thus, ϕ_s can be calculated as represented in the equation below:

$$\phi_s(i, j) = \phi_m(i, j) + \phi_r(i, j) \quad (4)$$

The displacement distribution can be derived by computing the difference in the distribution of the phase of patterns prior to and post-deformation. Phase differences ϕ_{m0} and ϕ_{m1} of the moiré pattern prior to and post-deformation are expressed as follows:

$$\phi_{m0} = \phi_{s0} - \phi_r \quad (5)$$

$$\phi_{m1} = \phi_{s1} - \phi_r \quad (6)$$

where ϕ_{s0} and ϕ_{s1} are phases of the grating pattern prior to and post-deformation, respectively. The phase difference $\Delta\phi_s$ of the grating pattern prior to and post-deformation can be found from the difference in phase between ϕ_{m0} and ϕ_{m1} , as follows:

$$\Delta\phi_s = \phi_{s1} - \phi_{s0} = \phi_{m1} - \phi_{m0} = \Delta\phi_m \quad (7)$$

(Equations were adapted from [23]).

Then, Equation (3) was used, and the displacement u and strain ε of the specimen grating can be obtained in the equations below.

$$u = p \frac{\Delta\phi_m}{2\pi} = -p \frac{\Delta\phi_s}{2\pi} \quad (8)$$

$$\varepsilon = \frac{du}{dx} = \frac{p}{2\pi} \frac{d(\Delta\phi_m)}{dx} = -\frac{p}{2\pi} \frac{d(\Delta\phi_s)}{dx} \quad (9)$$

where p = the pitch of the grating. (Equations were adapted from [14]).

2.2. Instrumentation

The scheme was validated using the CMOS sensor Mars4072S-24uc model (Figure 2A) of sensor size 1/1.7" with a pixel resolution of 4000×3000 and a frame rate of 24 fps. The camera was directly connected to the computer using a USB cable and operated using its software, *icentral*, to capture photographs.

For the experiment, a Hikvision DS-2CE16D0T-IRF HD 1080P IR bullet camera (CCTV camera), with a 2-megapixel high-performance image sensor of 6 mm lens and a video frame rate of 25 fps, was used to capture video for the scheme. The videos were recorded in the DVR box and exported for further processing as shown in Figure 2B,C.

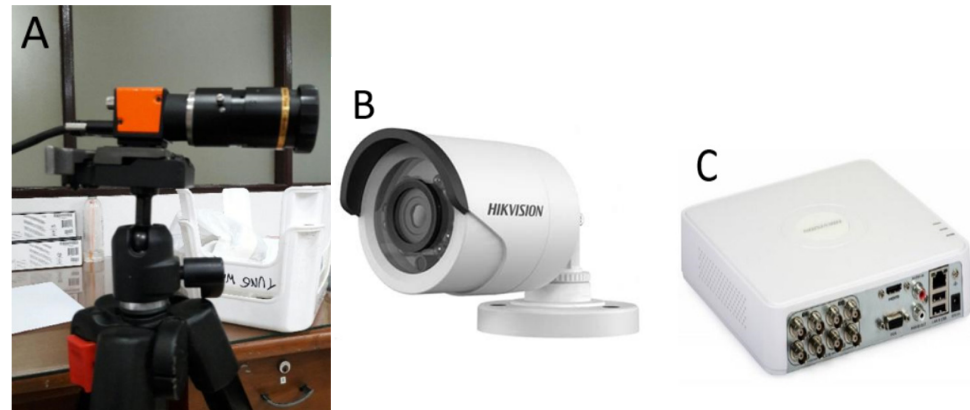


Figure 2. Photographs of the (A) CMOS sensor, (B) CCTV camera, and (C) DVR box.

Similarly, 2-D gratings of 4 mm, 2 mm, and 1 mm pitch were used as shown in Figure 3. The grating used for measurement requires constant pitch and a sharp variation of contrast. Initially, gratings printed on normal A4 paper using a laser printer were used. Later, these were printed on 4" \times 3" matte photo paper and finally upgraded to gratings printed at Amarin Printing and Publishing Public Company Limited, a publishing house, with 300 dpi on matte art paper by using a digital printing technique.

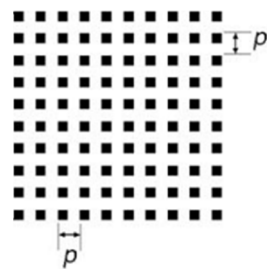


Figure 3. Two-dimensional grating [4].

The Matlab code for processing was prepared using the phase analysis method. It requires captured grating photographs as input. The phase difference of the grating before and after deformation provided the displacement values, the procedure of which was carried out as illustrated in Figure 4.

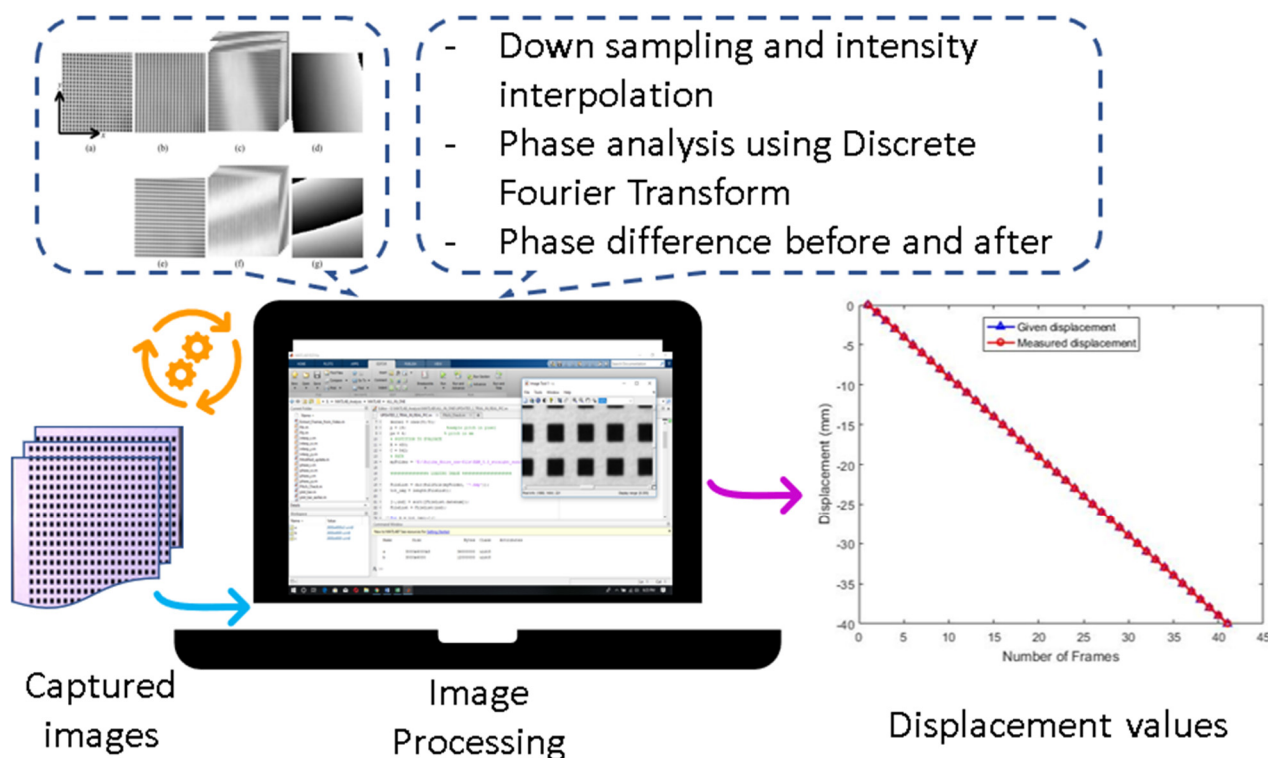


Figure 4. Diagram of the image processing of the captured images.

The sampling pitch in pixels and the position of the pixel at which the displacement is required are the input values used for processing. The sample pitch pixels were counted by observing the pixels that make up one pitch in the photograph.

2.3. Basic Setup

The general setup was such that the linear guide was used for displacing the grating. The grating, held inside the acrylic holder, was mounted on a linear guide secured by tape over the moving stage of the guide. This setup was arranged such that the grating was illuminated using two 50 W LED floodlights. The amount of displacement was controlled by the displacement transducer which was connected to a data logger. The moving stage was displaced at intervals of 1 mm and 0.5 mm in translation in the x-direction with to-and-fro motion using a displacement transducer.

2.4. Trial Experiments Using a CMOS Sensor

First, the suitability of the scheme was established with a series of trial experiments performed using CMOS sensor Mars and gratings of 4 mm and 2 mm pitch.

The first trial with a short tripod and A4-printed grating, and the second trial with a long tripod and matte photograph grating, were displaced at intervals of 1 mm to 0.25 mm for various cases. By corresponding the displacement values given to those measured using the code, the credibility of the code was assured.

2.5. Trial Experiments Using CCTV Camera

Sixteen cases were trialed for three setups with 4 mm-, 2 mm-, and 1 mm-pitch grating to determine a suitable pitch and distance for the experiment. The linear guide was displaced up to double the pitch in one direction and equal to the pitch in both directions for the experiment. The camera setup distances from the grating panel were maintained throughout the trials at distances of 5 cm, 10 cm, and 15 cm for 4 mm and 2 mm pitch and at 5 cm and 10 cm for 1 mm pitch. The trials differed in the improvements in the camera settings and the use of upgraded matte art grating.

All in all, 4 mm and 2 mm pitches delivered consistent outcomes and the distances of 10 mm or less seemed to work better. With the 1 mm pitch, the deviation values under the theoretical band of error were not achieved for all cases. The theoretical band of error is the $p/100$ th of the grating pitch for this method.

3. Experiment Conducted on The Specimen

The specimen used in the experiment is a steel I-beam which is 1170 mm long. The span between the two supports was 1000 mm. The total height and width of the beam were 150 mm each. The web was 7 mm thick while the flange was 10 mm thick.

3.1. Experimental Setup

An asymmetric three-point bending test was performed on the specimen to measure the deflection at the point of loading and determine the strain values. The displacement transducers were located at the bottom flange of the beam at a distance of $L/4$ th of the way along the span, as seen in Figure 5. The gratings were also pasted on wooden panels at the same positions facing the array of three cameras. Eight strain gauges were installed such that four were laid on either side of the mid-span between the $L/4$ th positions, as shown in Figure 6. The specimen was loaded at the middle of the beam by a loading frame of 15 tons of capacity.

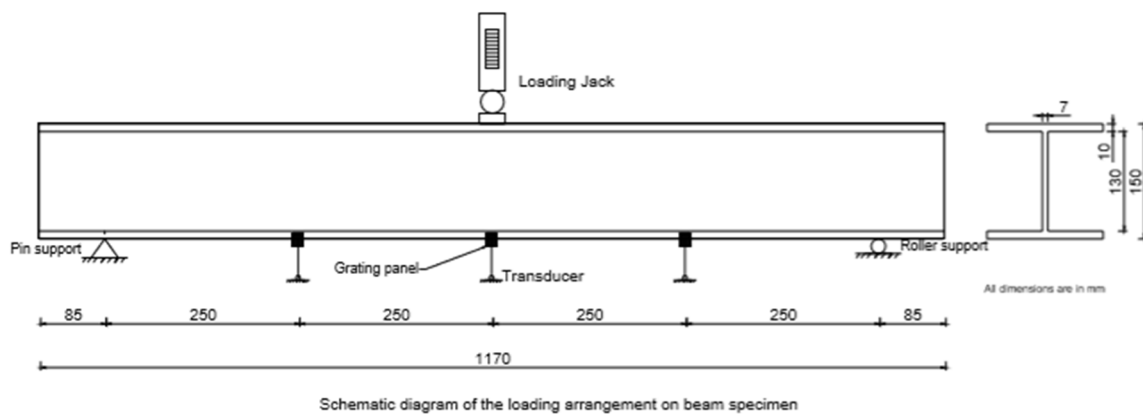


Figure 5. Schematic diagram of the experiment.

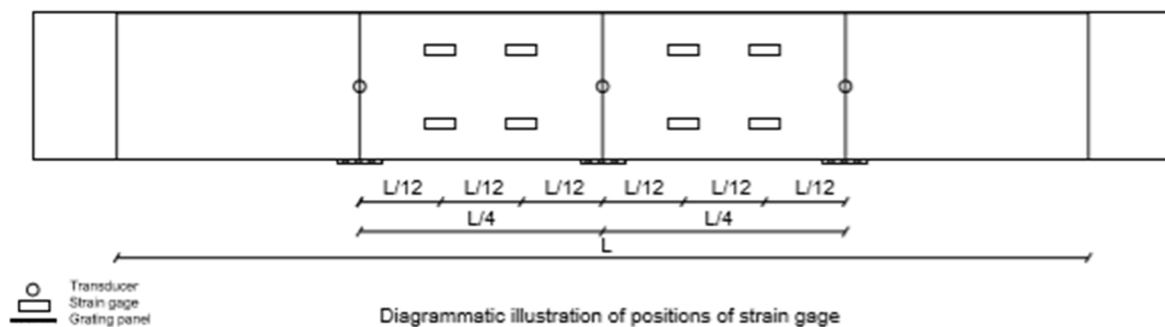


Figure 6. Schematic designations of the instruments on the beam.

In the experiment, Figure 7, 4 mm and 2 mm gratings were used to capture the x-direction and y-direction displacement simultaneously from the array of cameras. The CCTV cameras were kept at a 10 cm distance from position A and position C and at a 5 cm distance from position B. The sample was pre-loaded at 1 ton at the center of the top flange of the sample with the load cell at every 0.5-ton interval up to 8 tons and unloaded back to the pre-loaded position. The displacement values were analyzed at the pixel at which the $L/4$ th position of the specimen was marked on the grating panel, as seen in Figure 8.



Figure 7. Photograph of the experimental setup in a specimen with labels. (1) Loading cell, (2) I-beam specimen, (3) grating panel, (4) linear guide (5) CCTV camera, (6) monitor for operating the camera, (7) DVR box, (A–C) camera positions.

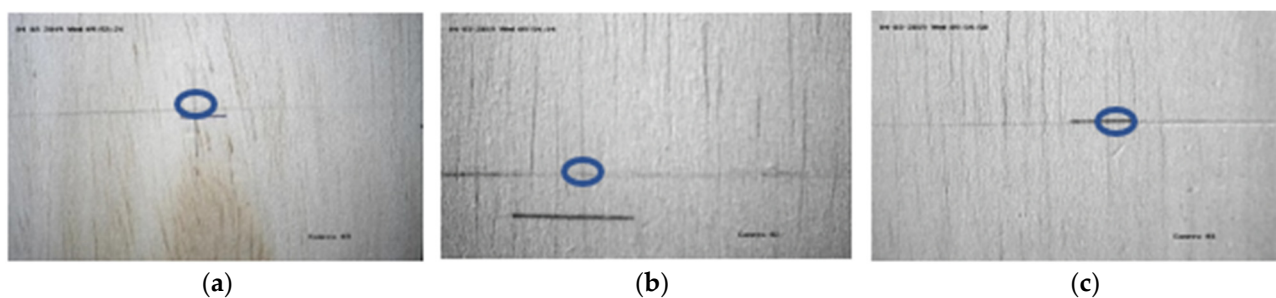
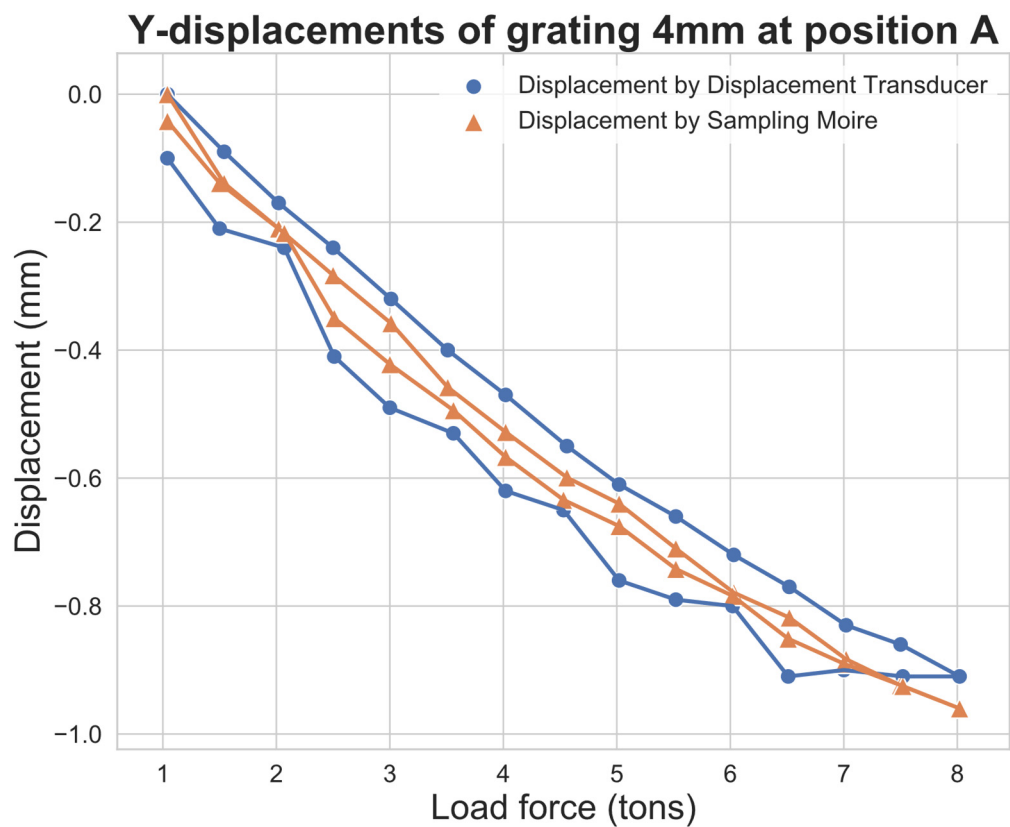


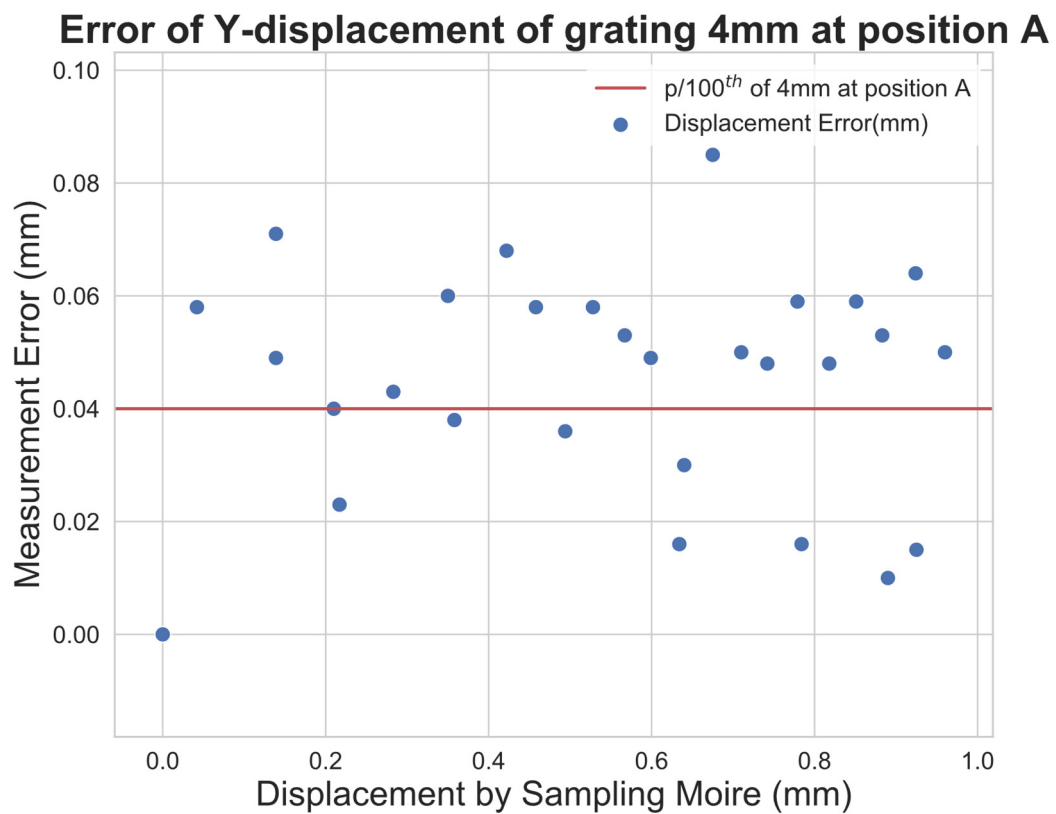
Figure 8. Photographs showing the pixel position (column, row) at which the analysis was performed for the cameras. (a) At A (433, 233), (b) at B (335, 374), (c) at C (542, 256).

3.2. Displacement Measurement

Overall, the RMS error calculation revealed that irrespective of distance, the average resolution of $55\ \mu$ and $35\ \mu$ was obtained for 4 mm grating and 2 mm grating, respectively. The first graph for each position from Figures 9–14 show us how the displacement values vary over loading and unloading in both methods, while the graph comparing each position from Figures 9–14 show the variation of error values that are within the $p/100$ th of grating pitch and the ones that exceed. Similarly, the plot of the comparison of displacement values by both the sampling moiré method and the displacement transducer shows a good degree of correlation.



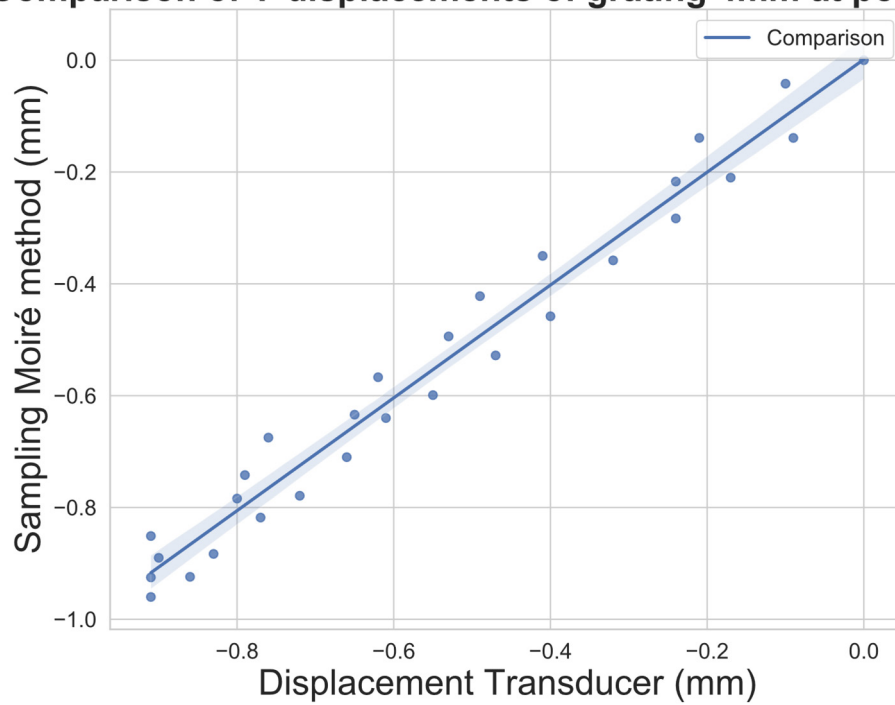
(a)



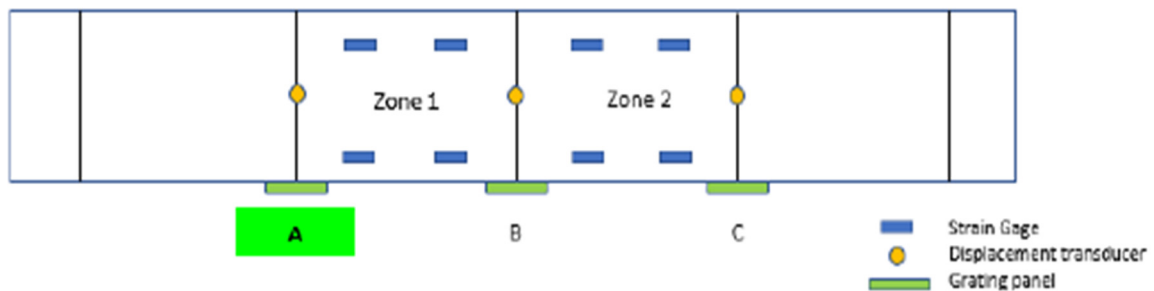
(b)

Figure 9. Cont.

Comparison of Y-displacements of grating 4mm at position A



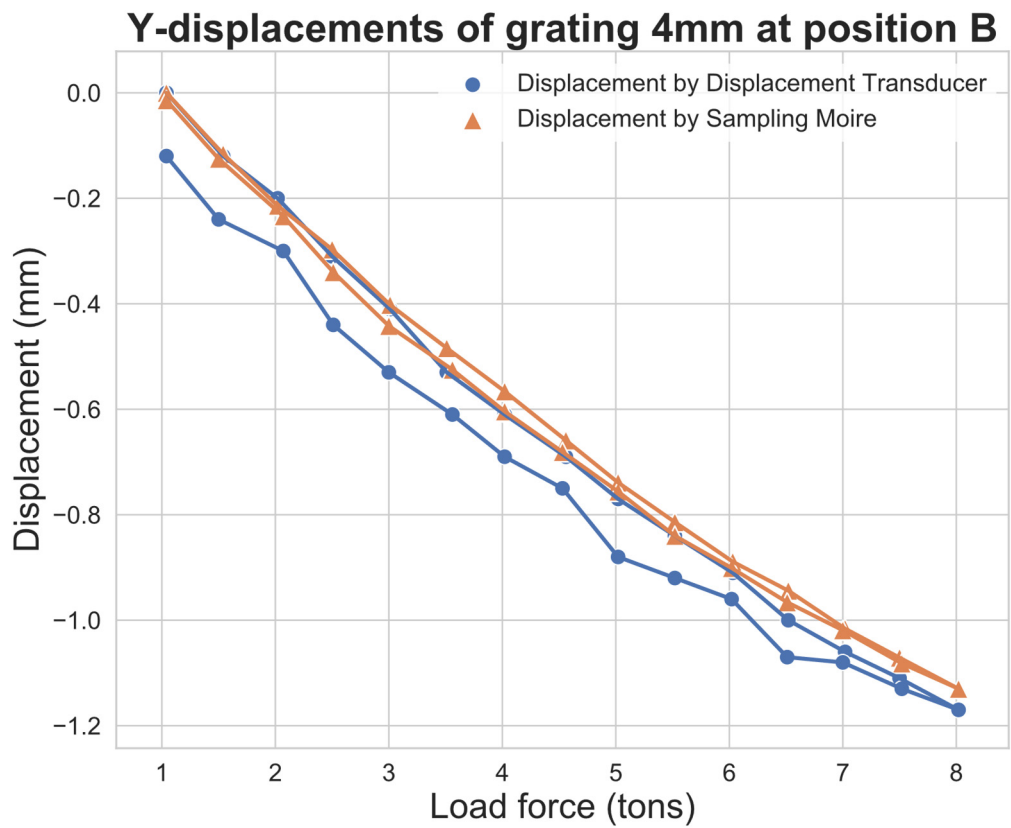
(c)



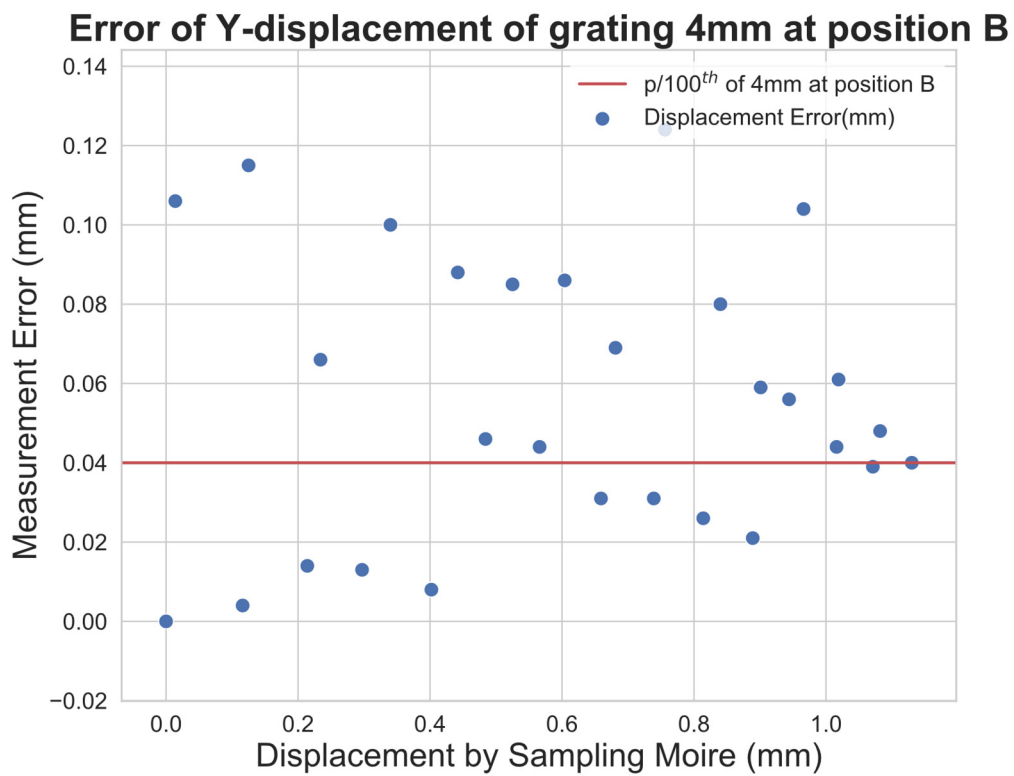
RMS Error	0.0491 mm
Minimum Error	0.0101 mm
Maximum Error	0.0851 mm
Average Error	0.0450 mm

(d)

Figure 9. Various graph plots for displacement values (coefficient correlation = 0.985) by the displacement transducer and the sampling moiré method and their derivatives at camera position A for 4 mm grating. (a) Force–displacement, (b) displacement and measurement error, (c) displacement and sampling, (d) position A of the beam.



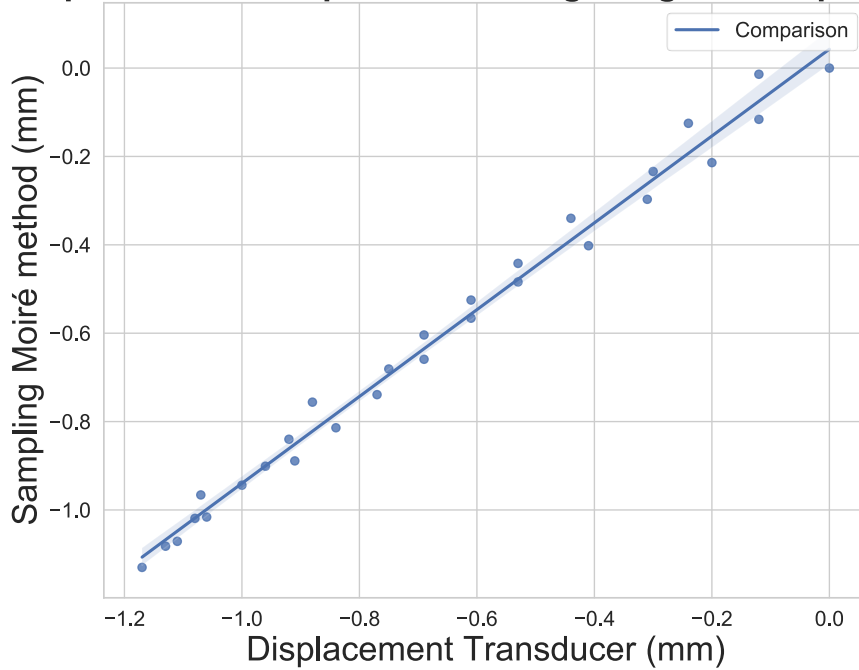
(a)



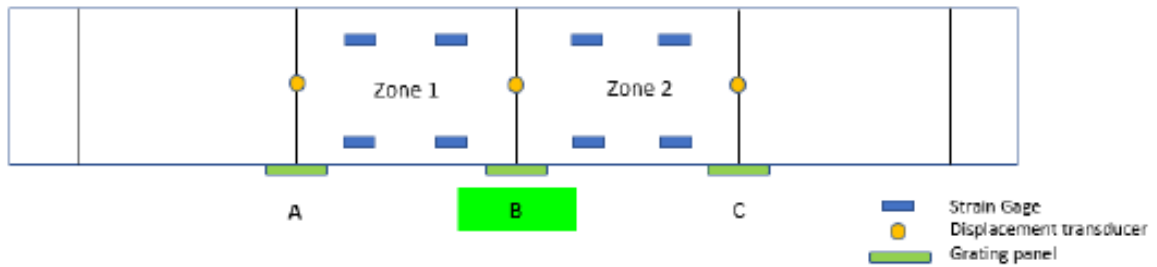
(b)

Figure 10. Cont.

Comparison of Y-displacements of grating 4mm at position B



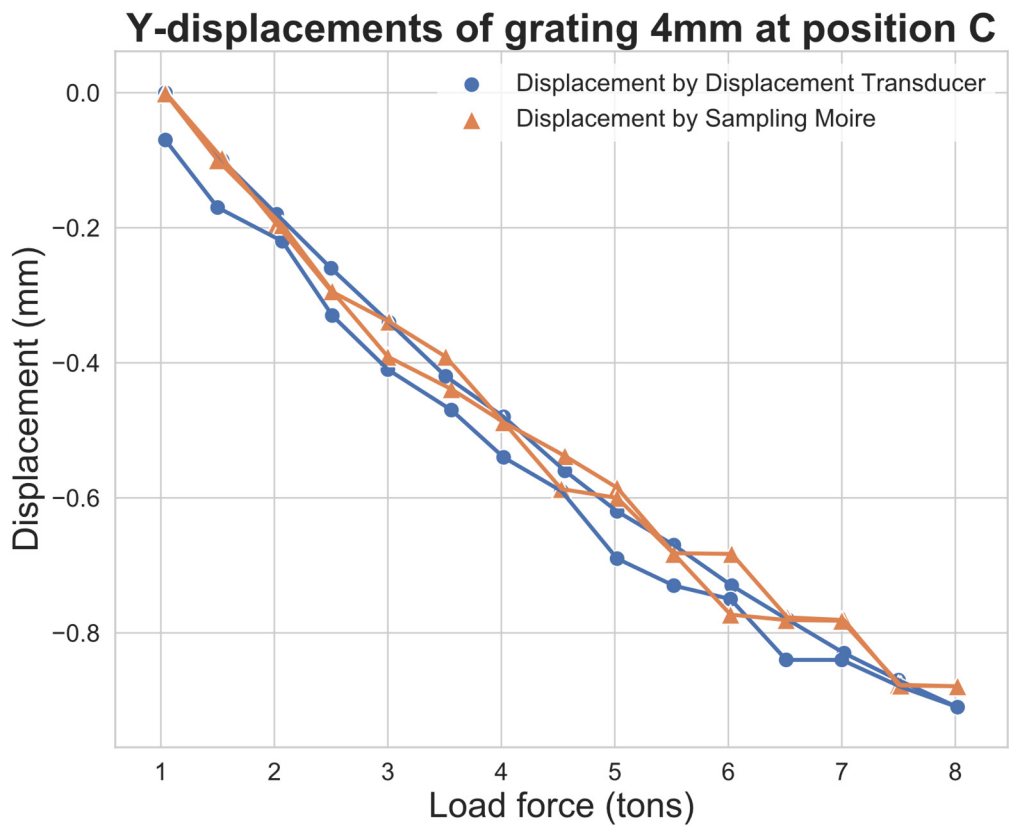
(c)



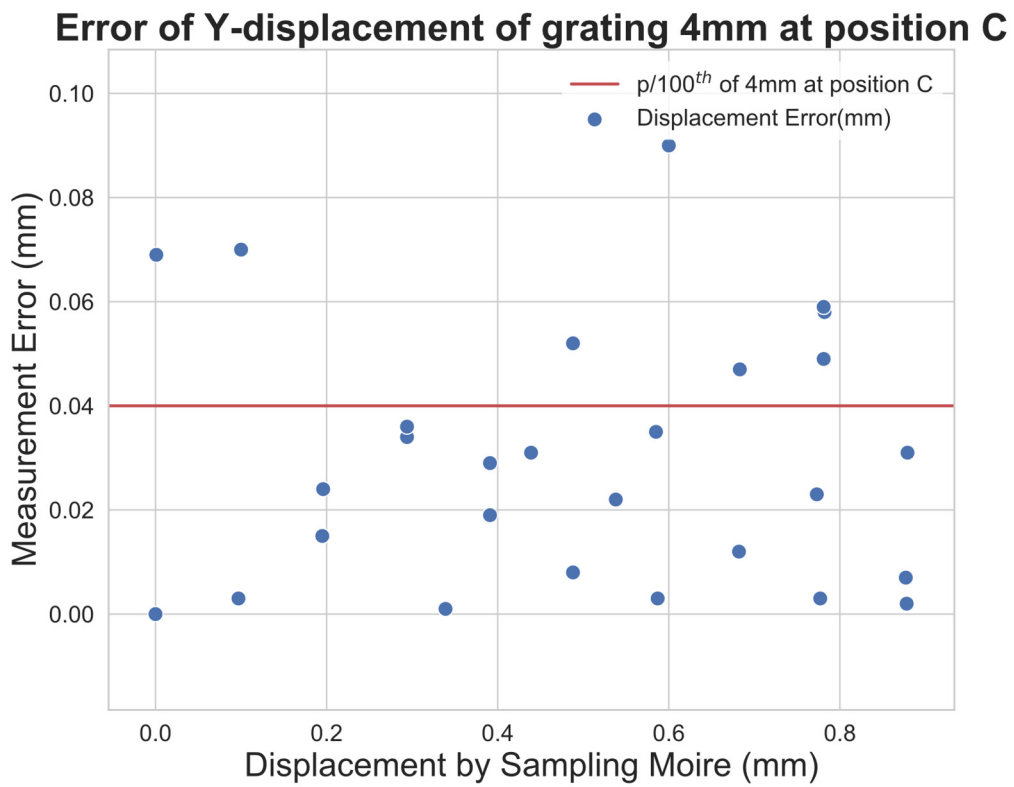
RMS Error	0.0653 mm
Minimum Error	0.0044 mm
Maximum Error	0.1240 mm
Average Error	0.0555 mm

(d)

Figure 10. Various graph plots for displacement values (coefficient correlation = 0.9945) by the displacement transducer and the sampling moiré method and their derivatives at camera position B for 4 mm grating. (a) Force–displacement, (b) displacement and measurement error, (c) displacement and sampling, (d) position B of the beam.



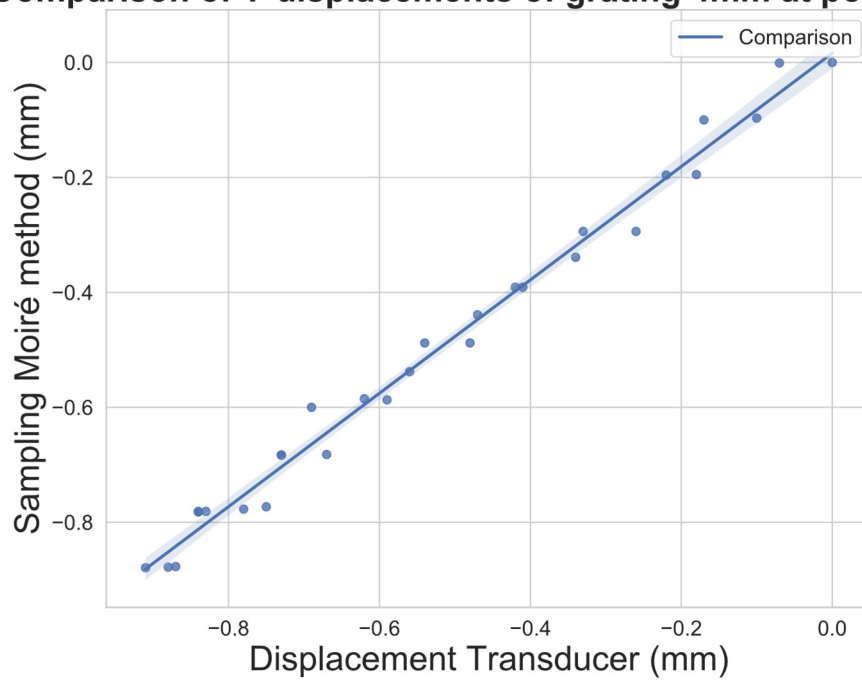
(a)



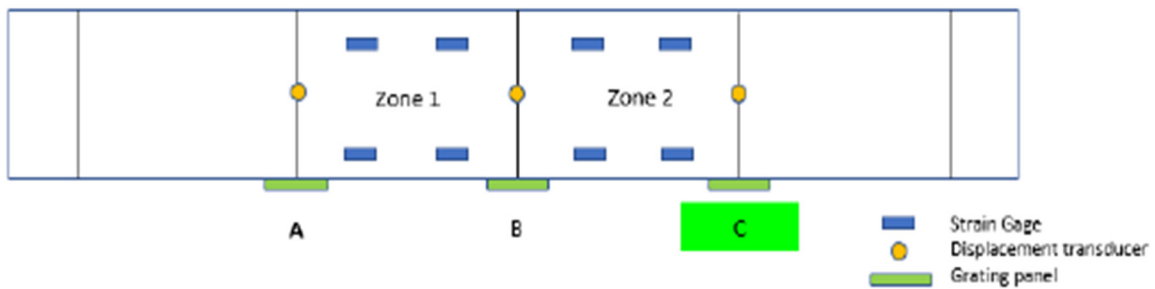
(b)

Figure 11. Cont.

Comparison of Y-displacements of grating 4mm at position C



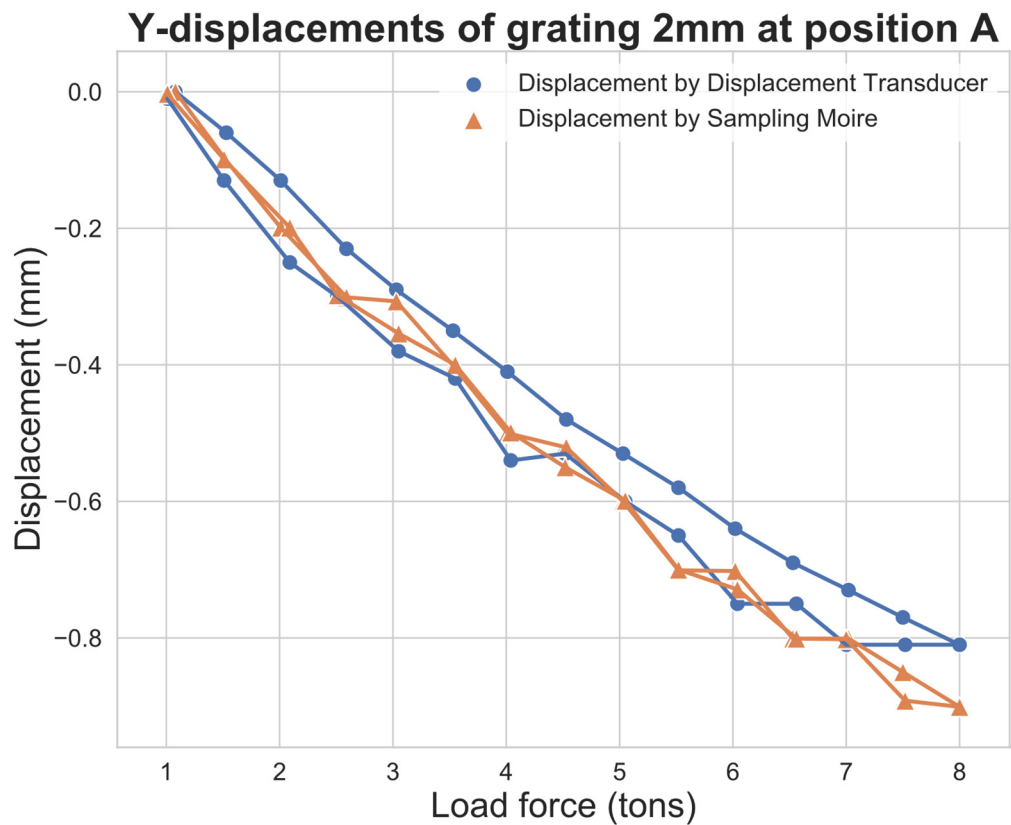
(c)



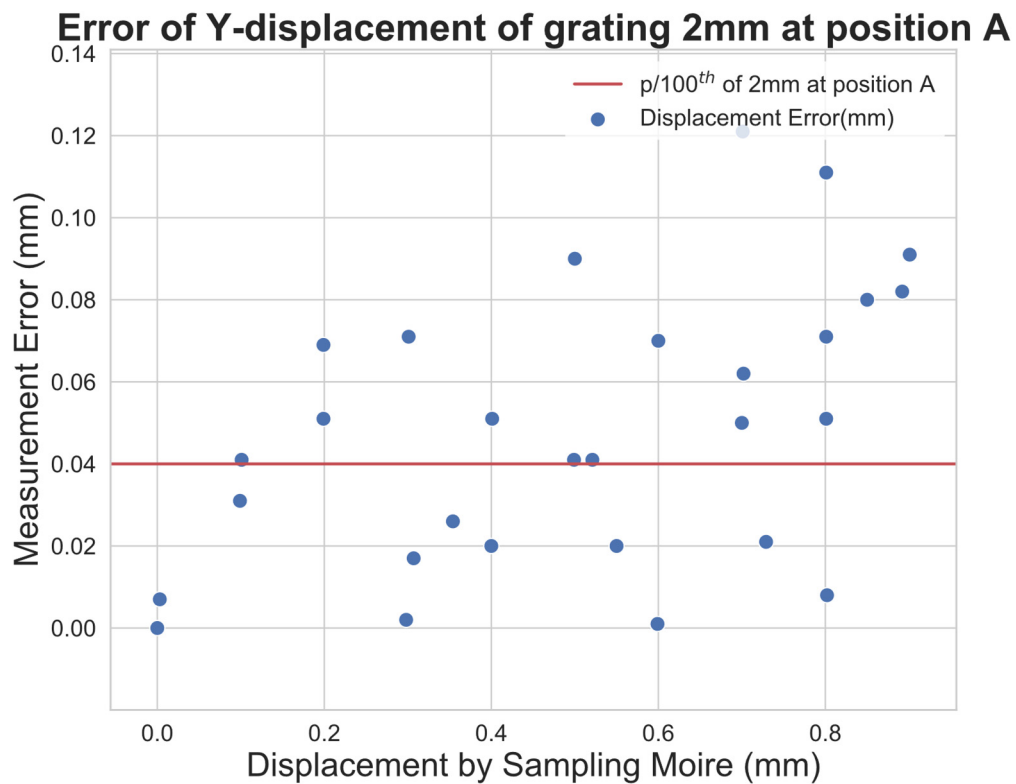
RMS Error	0.0385 mm
Minimum Error	0.0009 mm
Maximum Error	0.0902 mm
Average Error	0.0303 mm

(d)

Figure 11. Various graph plots for displacement values (coefficient correlation = 0.9936) by the displacement transducer and the sampling moiré method and their derivatives at camera position C for 4 mm grating. (a) Force–displacement, (b) displacement and measurement error, (c) displacement and sampling, (d) position C of the beam.



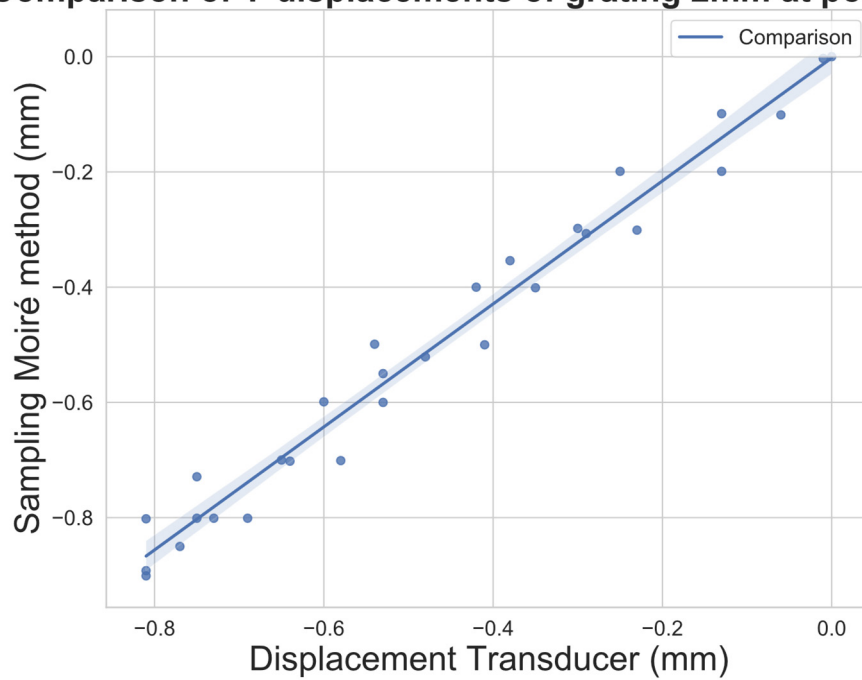
(a)



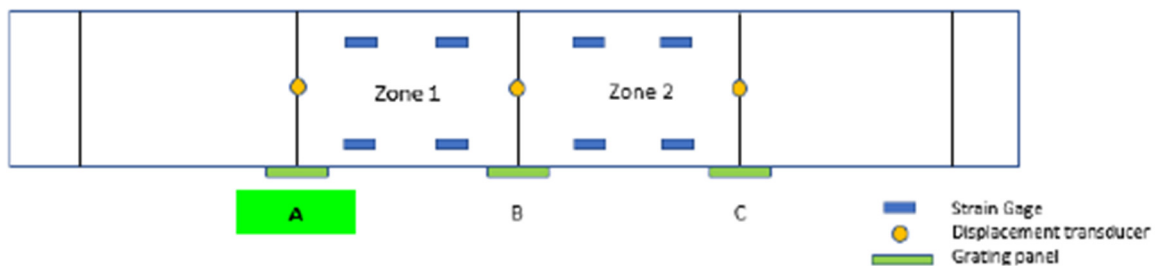
(b)

Figure 12. Cont.

Comparison of Y-displacements of grating 2mm at position A



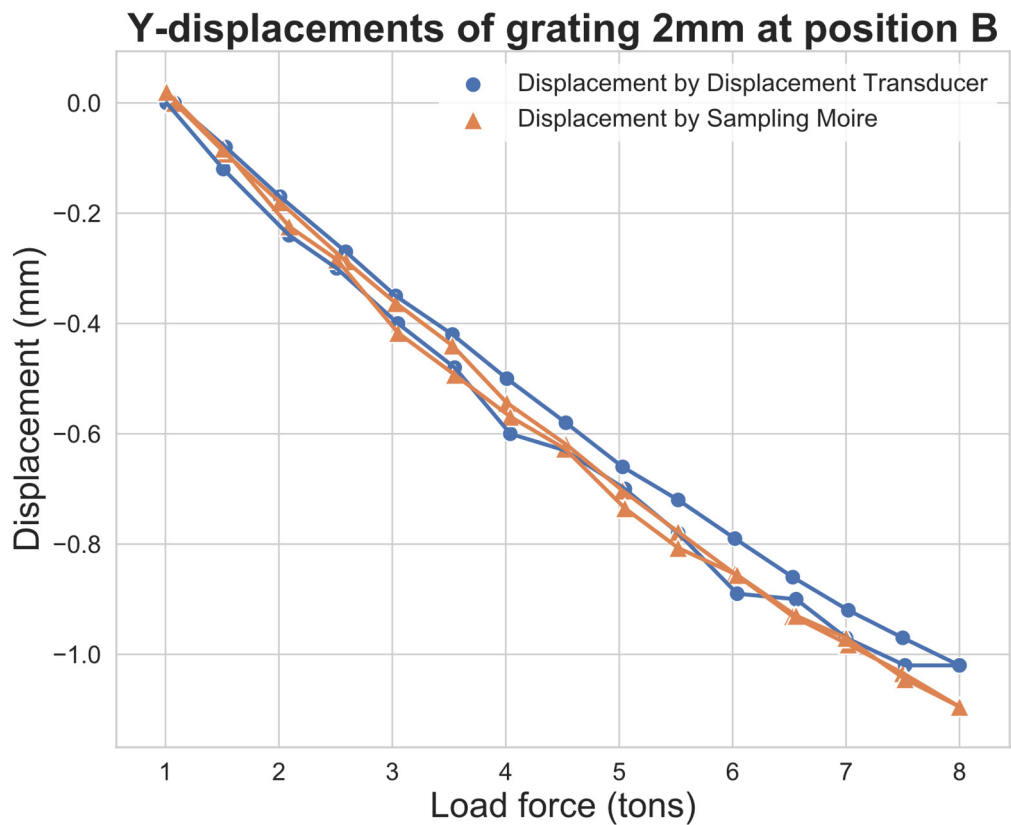
(c)



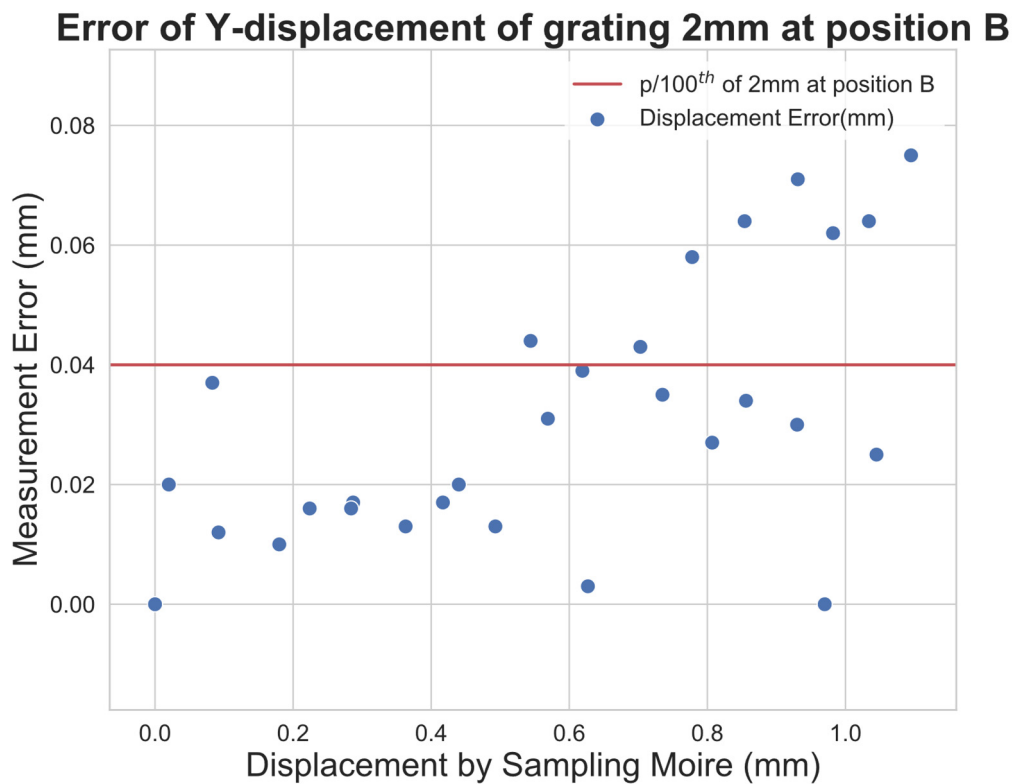
RMS Error	0.0583 mm
Minimum Error	0.0006 mm
Maximum Error	0.1209 mm
Average Error	0.0481 mm

(d)

Figure 12. Various graph plots for displacement values (coefficient correlation = 0.9866) by the displacement transducer and the sampling moiré method and their derivatives at camera position A for 2 mm grating. (a) Force–displacement, (b) displacement and measurement error, (c) displacement and sampling, (d) position A of the beam.



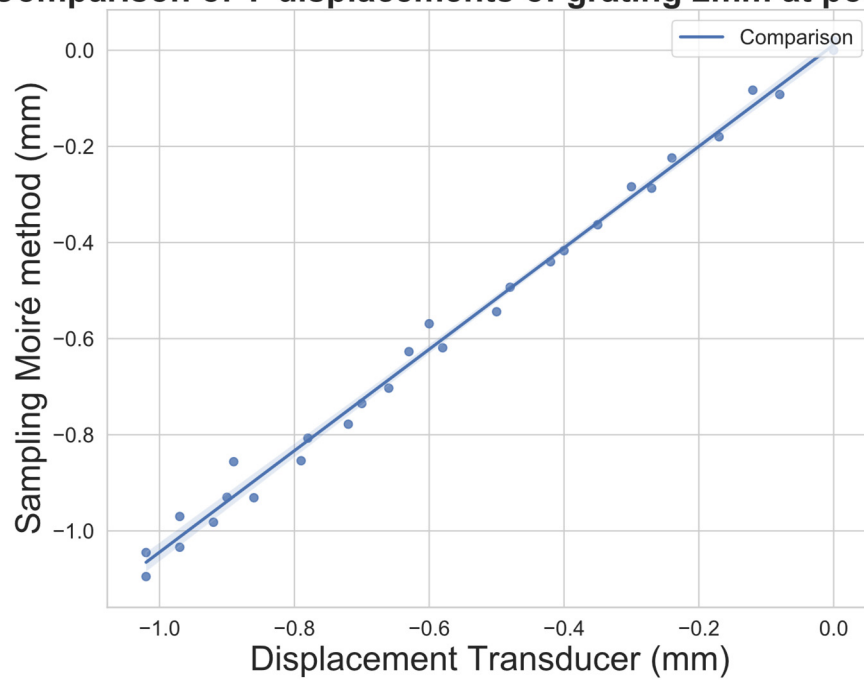
(a)



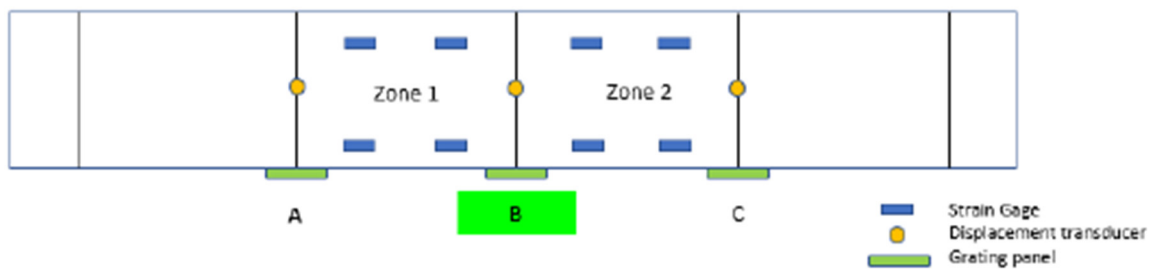
(b)

Figure 13. Cont.

Comparison of Y-displacements of grating 2mm at position B



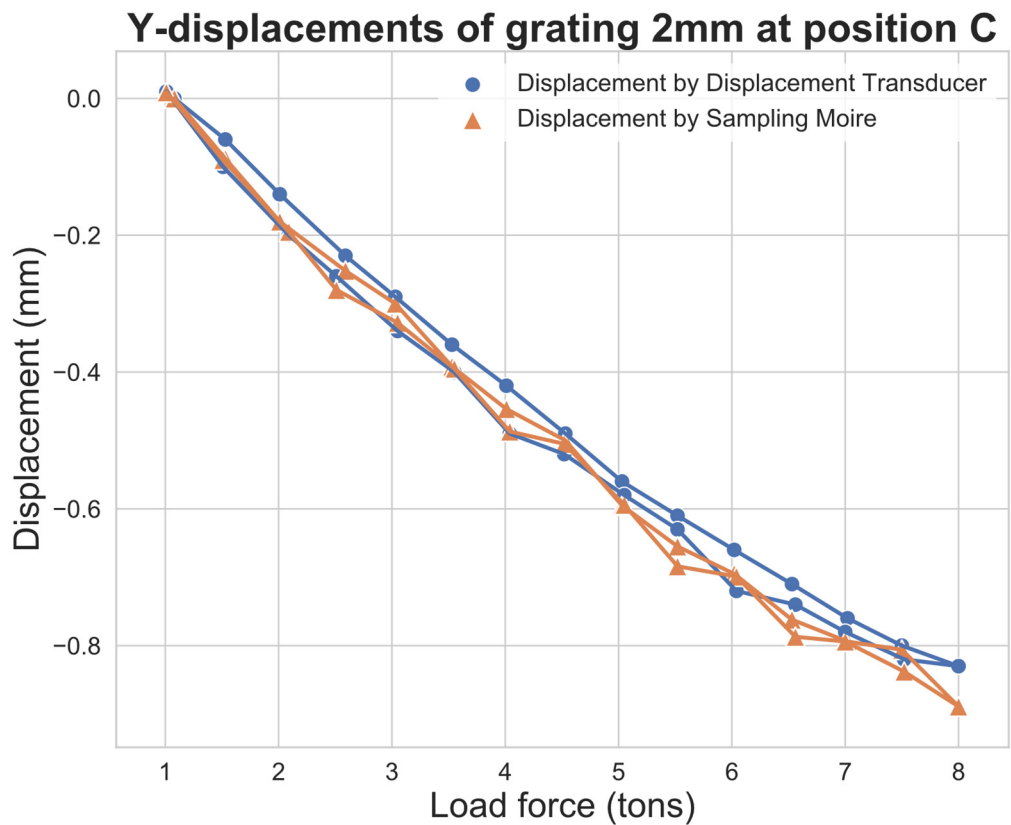
(c)



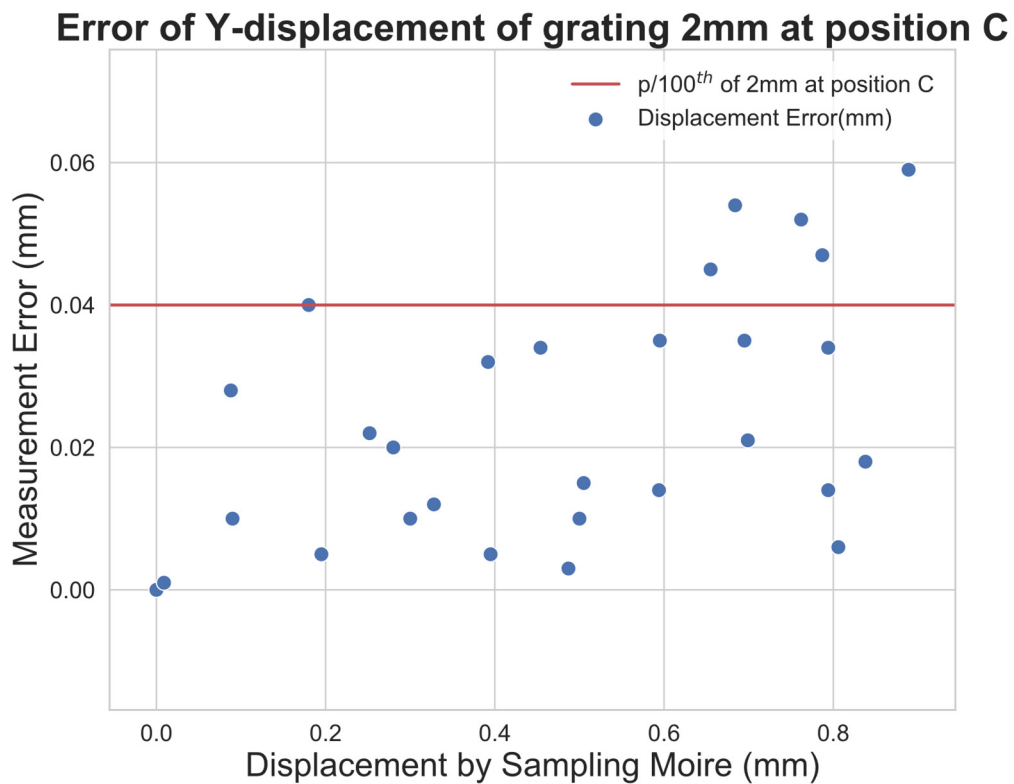
RMS Error	0.0377 mm
Minimum Error	0.0003 mm
Maximum Error	0.0752 mm
Average Error	0.0310 mm

(d)

Figure 13. Various graph plots for displacement values (coefficient correlation = 0.9969) by the displacement transducer and the sampling moiré method and their derivatives at camera position B for 2 mm grating. (a) Force–displacement, (b) displacement and measurement error, (c) displacement and sampling, (d) position B of the beam.



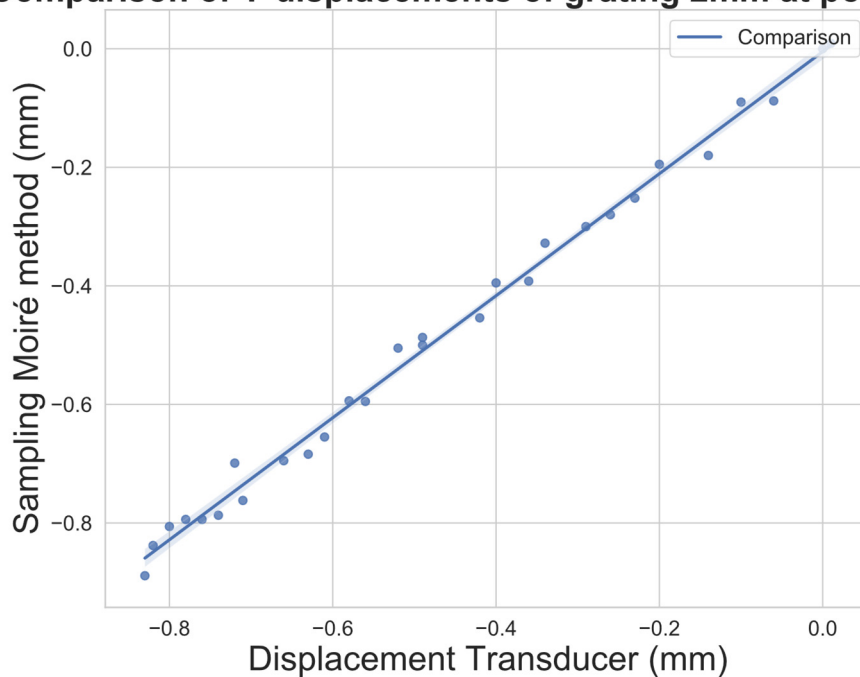
(a)



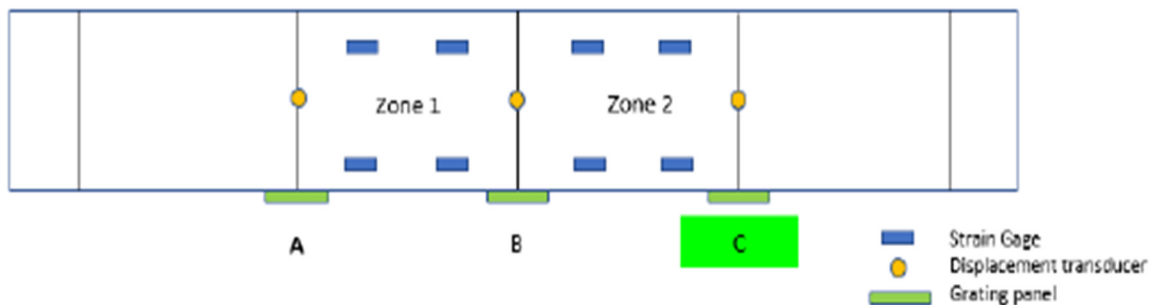
(b)

Figure 14. Cont.

Comparison of Y-displacements of grating 2mm at position C



(c)



RMS Error	0.0289 mm
Minimum Error	0.0008 mm
Maximum Error	0.0589 mm
Average Error	0.0234 mm

(d)

Figure 14. Various graph plots for displacement values (coefficient correlation = 0.997) by the displacement transducer and the sampling moiré method and their derivatives at camera position C for 2 mm grating. (a) Force–displacement, (b) displacement and measurement error, (c) displacement and sampling, (d) position C of the beam.

3.3. Strain Measurement

Strain is the deformation incurred in a solid when stress is produced on it due to the application of force. Therefore, strain is the amount of deformation per unit of its original length.

$$\text{Here, strain } (\epsilon) = \frac{\text{relative change in x - displacement } (\Delta l)}{\text{gauge length } (L_0)}$$

Strain gauges of gauge length 5 mm and resolution $1 \mu\epsilon$ were installed at certain locations, as seen in Figure 6. Thus, a 25 mm gauge length (as in this case), would require a

0.025 μm resolution for displacement measurement. If $p/100$ th of the grating was taken to be 0.025 μm , the size of the grating would be 2.5 μm , which is too small and would require the nano-printing of the grating pitch.

3.4. Outcome of the Measurement Scheme and its Limitations

Taking a conservative approach, even if the fluctuation of 10% of the maximum strain is allowed, a 0.25 μm resolution is needed, which is still small. The inherent amount of error in the current scheme is 186 $\mu\epsilon$. In the results, the x-displacement is towards the left and thus all the values tend to be negative. The plot henceforth is carried out taking solely magnitude.

The average strain gauge values agree better through both conditions for Zone 2 and lags for loading conditions for Zone 1. However, the calculated strain values do not follow the pattern of the averaged values for either zone, as seen from the third figure of the graphs. From the second graph in each of Figures 15–18, it is seen that Zone 2 captured the tentative pattern better, as is evident from the R-squared value of the 4 mm grating. All things considered, the RMS error has not exceeded the error of the measurement scheme of 186 $\mu\epsilon$.

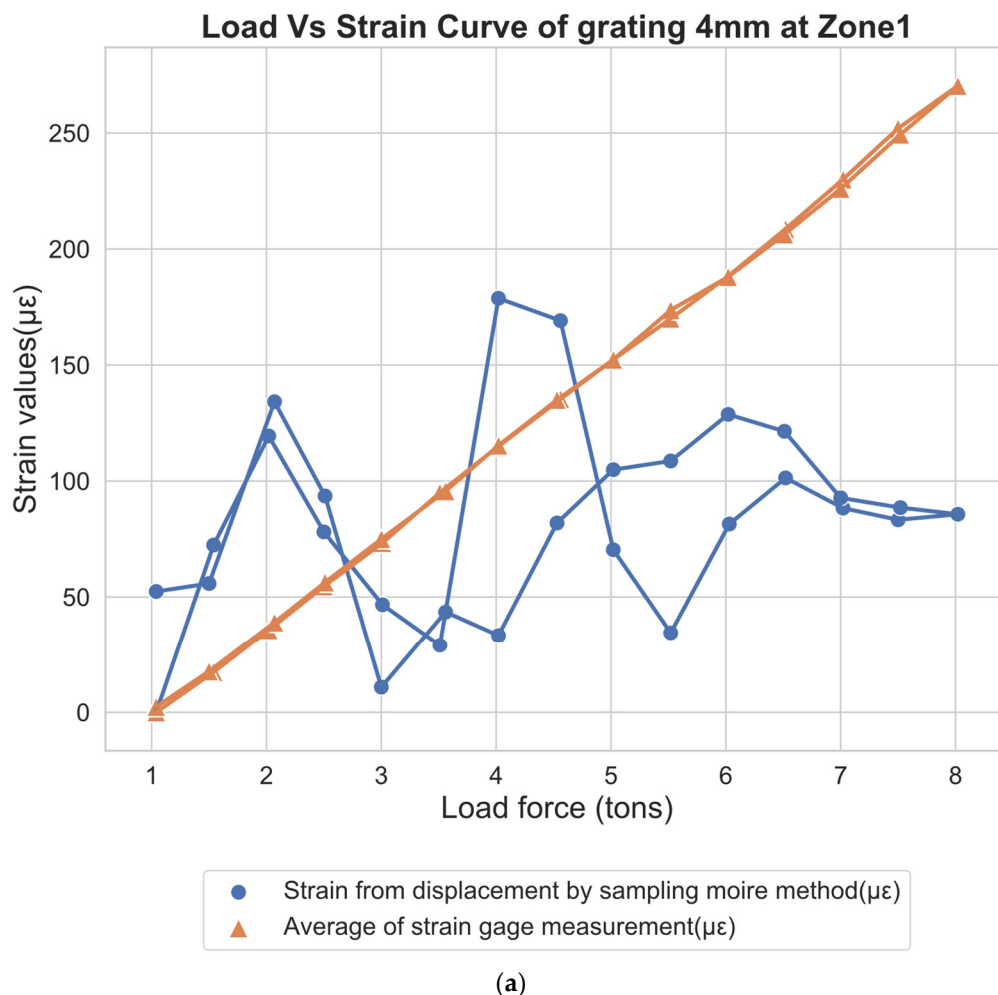


Figure 15. Cont.

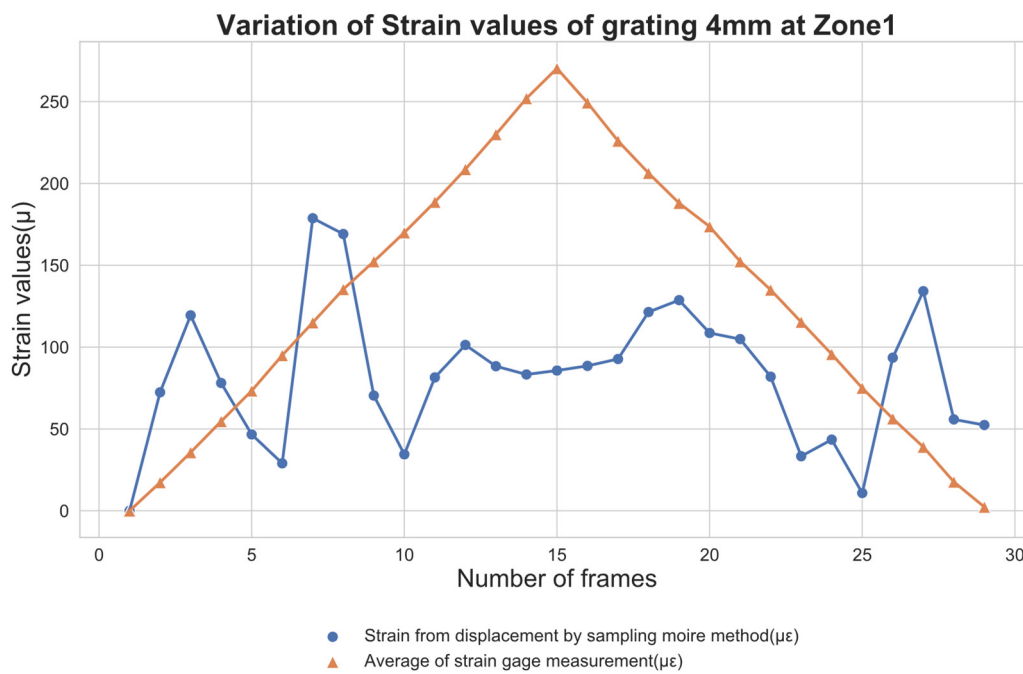
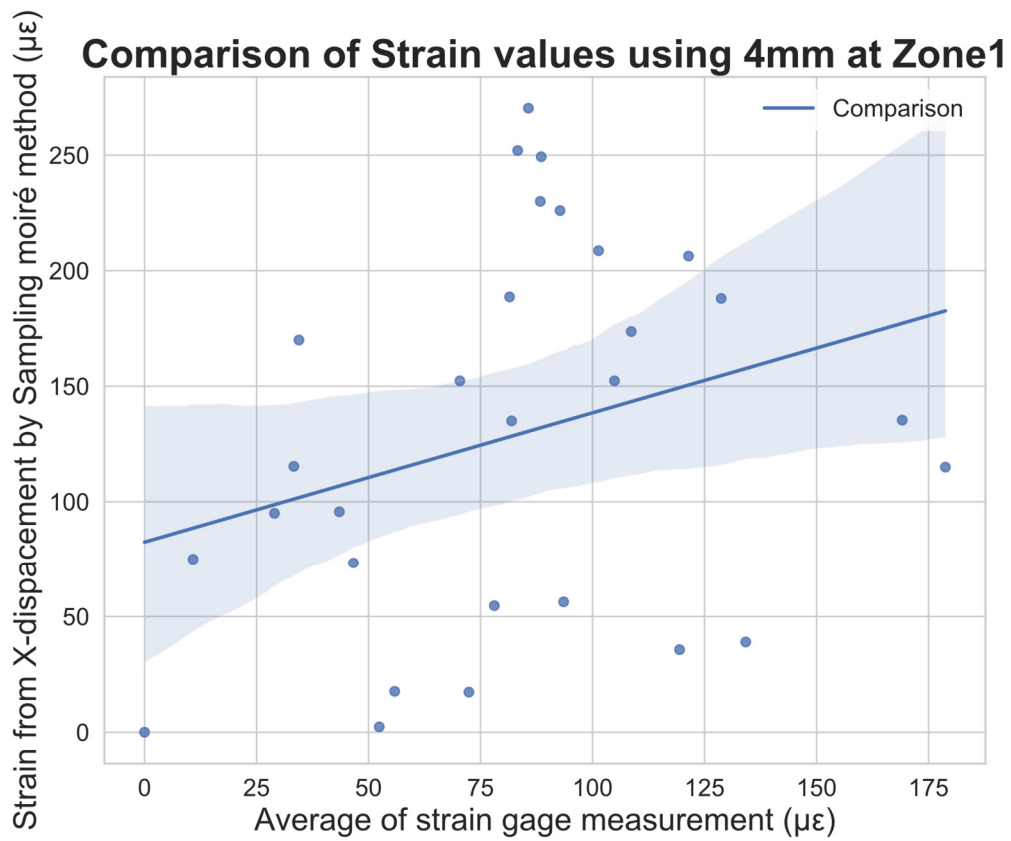


Figure 15. Cont.

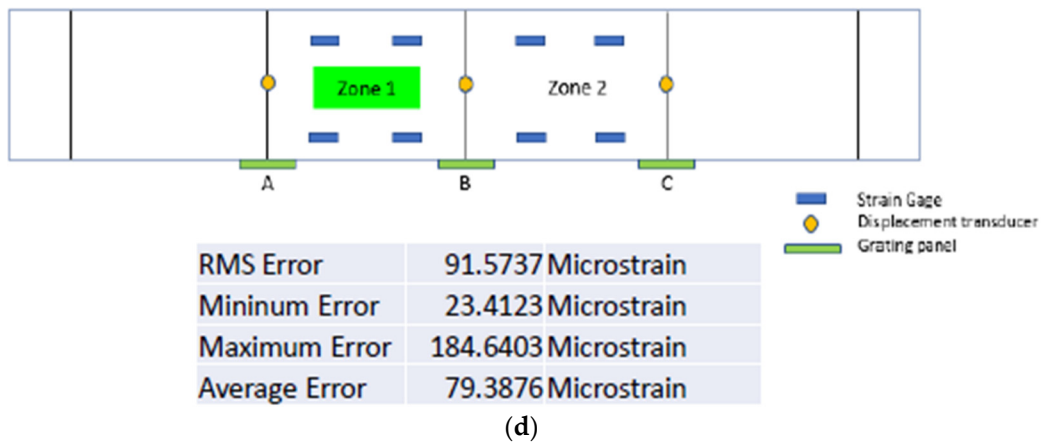


Figure 15. Various graph plots for strain values (coefficient correlation = -0.291) by strain gauge and the sampling moiré method and their derivatives for Zone 1 using 4 mm grating. (a) Force–strain, (b) average of strain gauge and measured strain, (c) number of frames and strains, (d) position of Zone 1 of the beam.

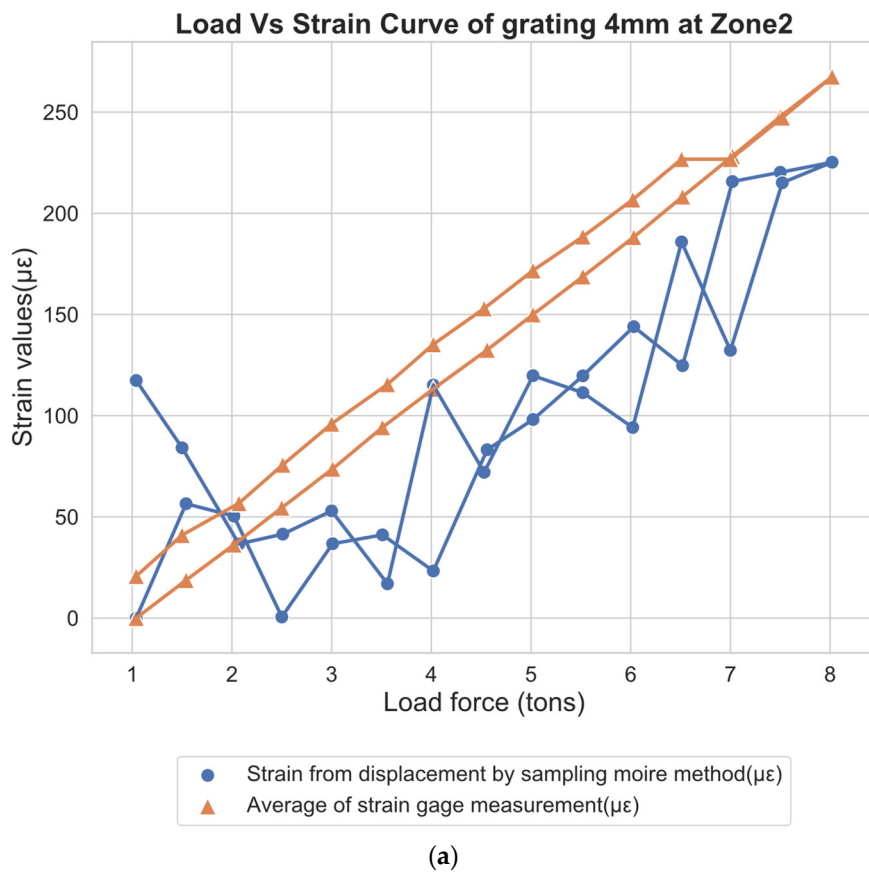


Figure 16. Cont.

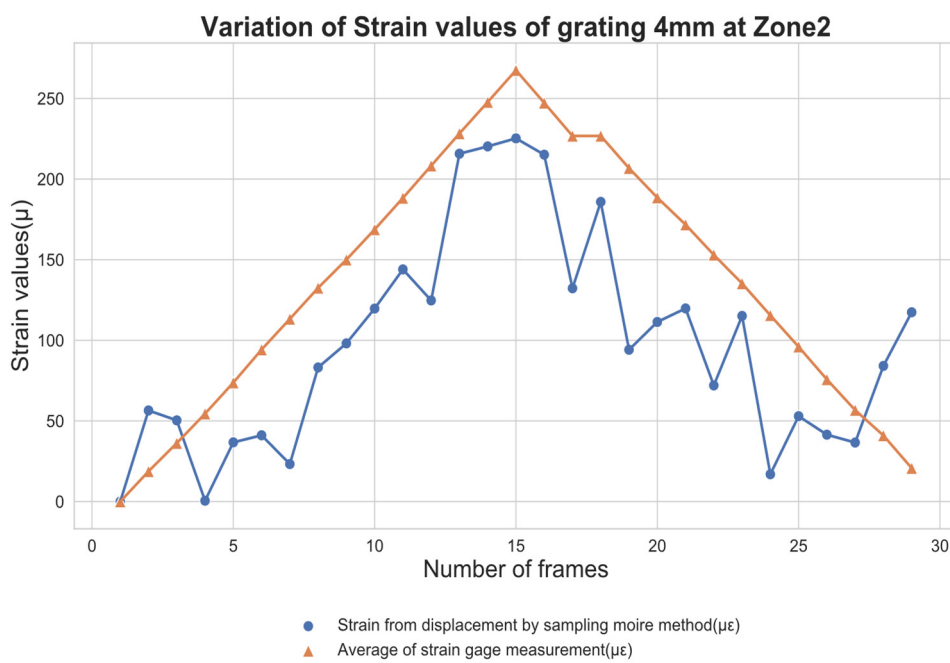
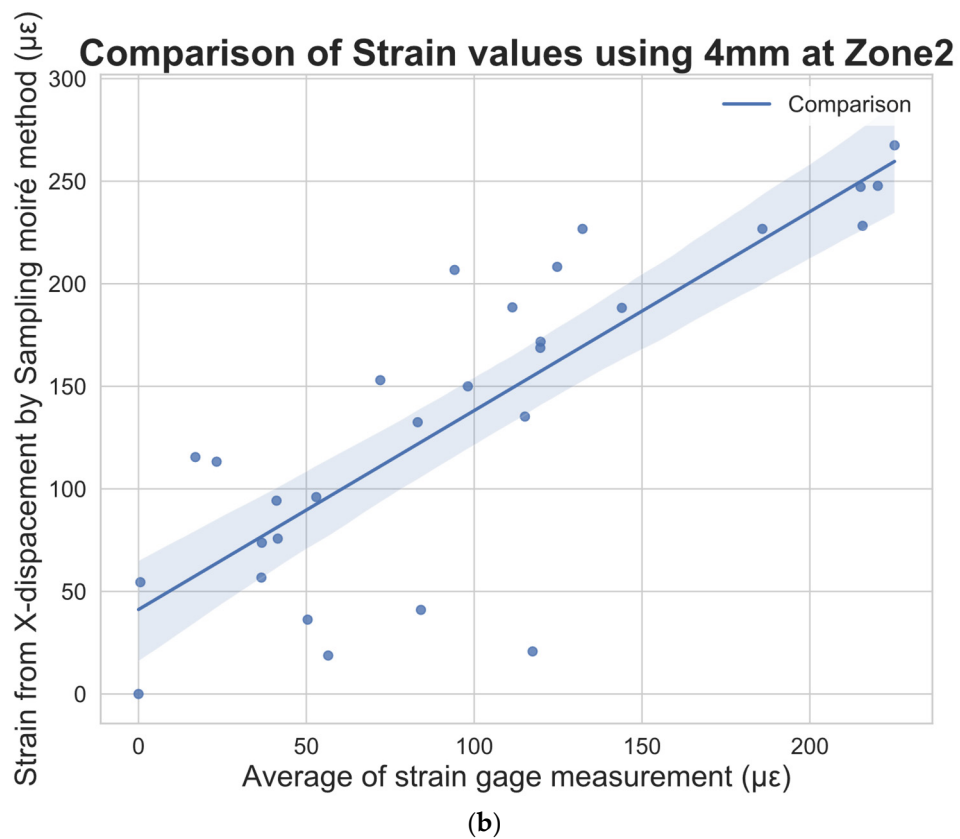


Figure 16. Cont.

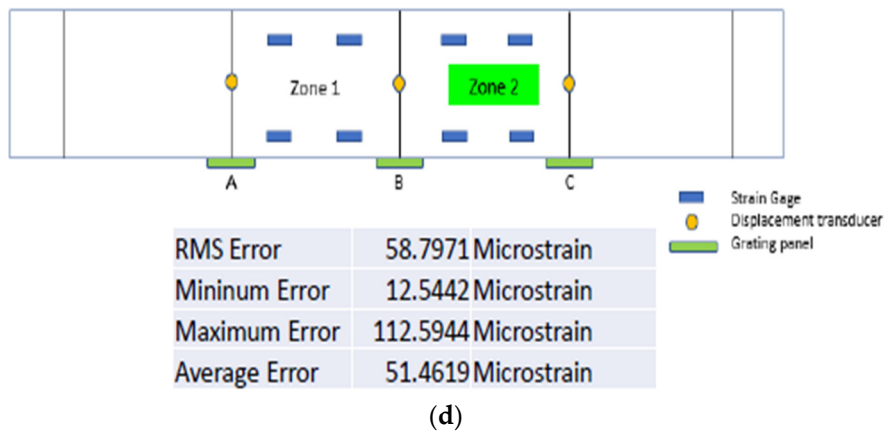


Figure 16. Various graph plots for strain values (coefficient correlation = -0.8181) by strain gauge and the sampling moiré method and their derivatives for Zone 2 using 4 mm grating. (a) Force–strain, (b) average of strain gauge and measured strain, (c) number of frames and strains, (d) position of Zone 2 of the beam.

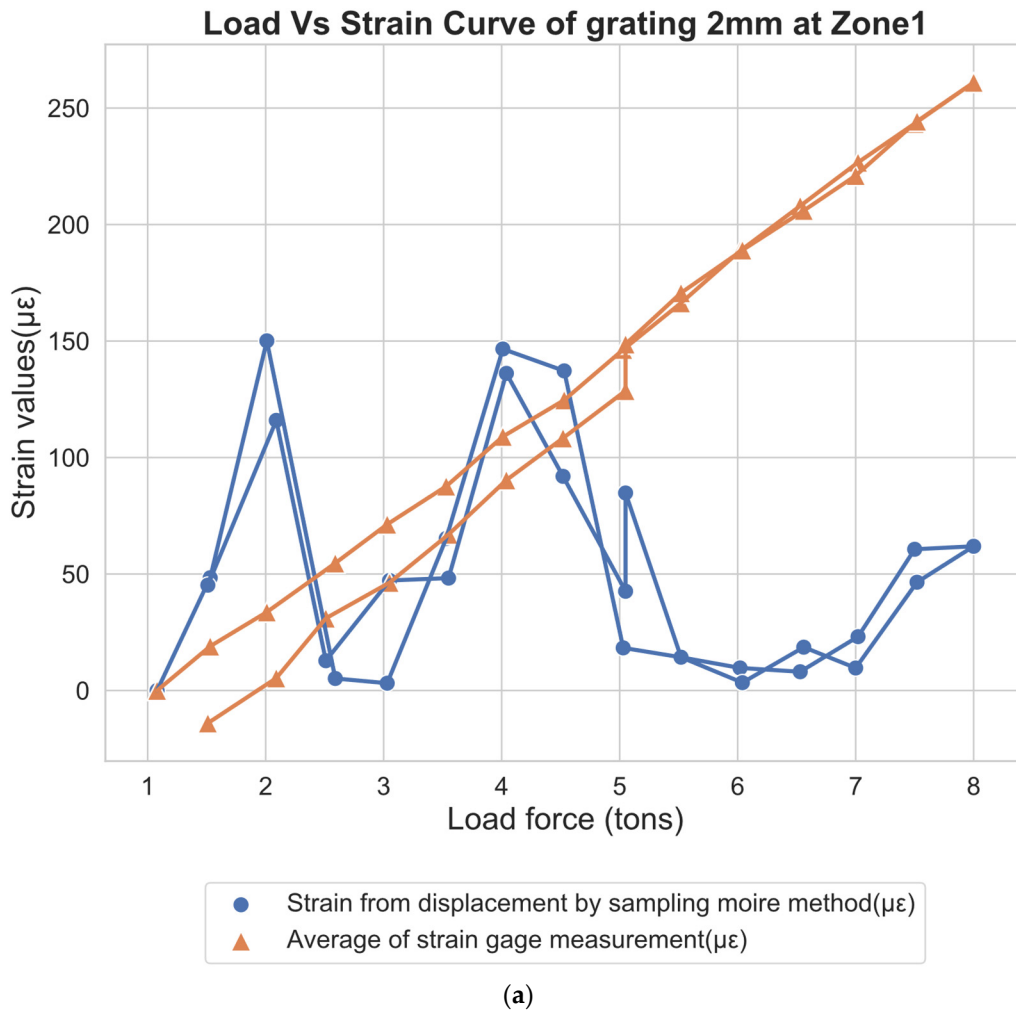


Figure 17. Cont.

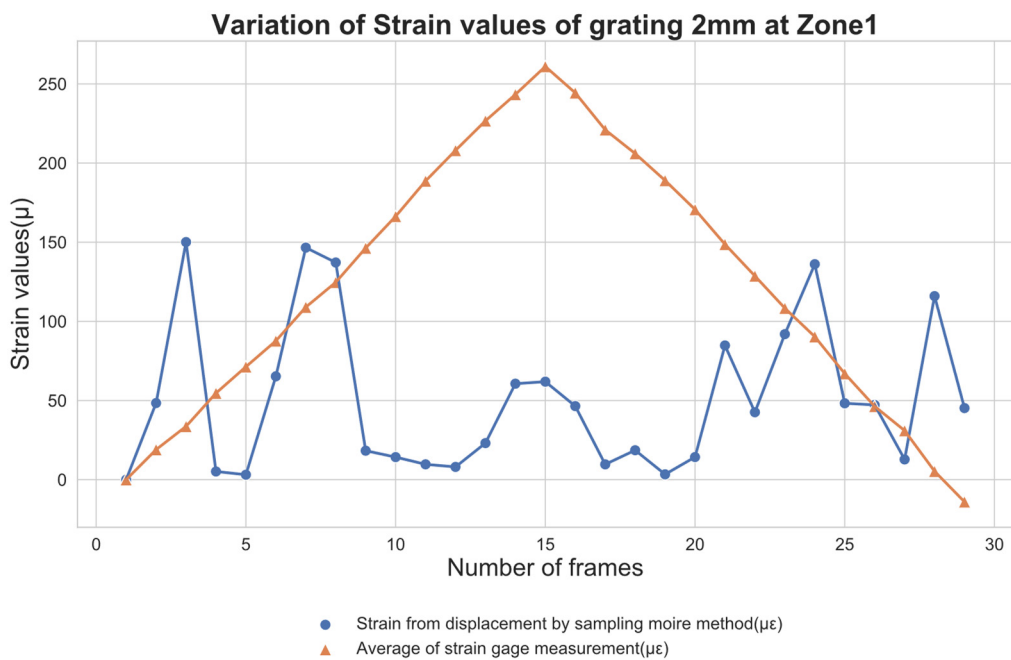
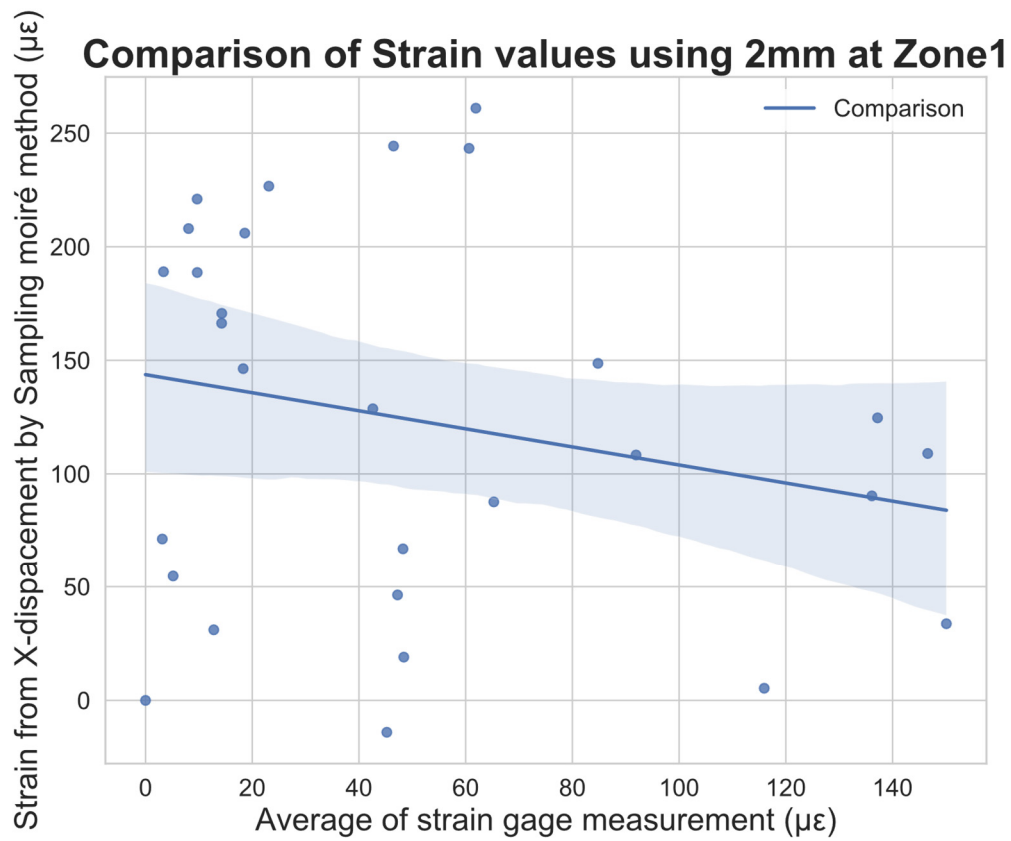


Figure 17. Cont.

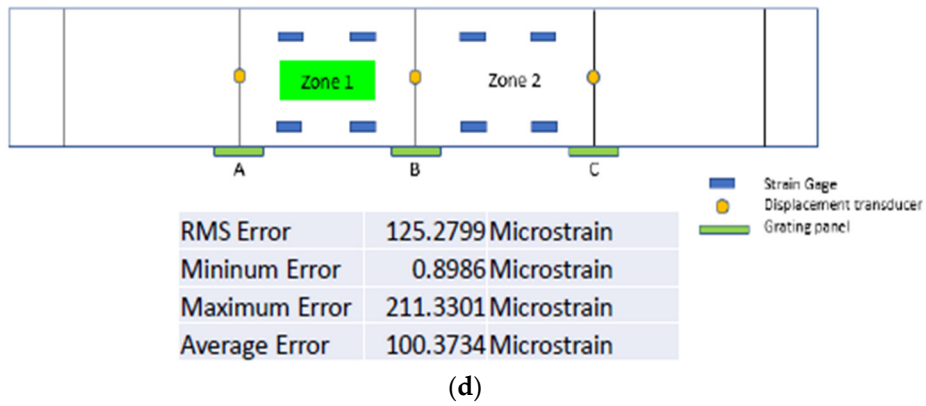


Figure 17. Various graph plots for strain values (coefficient correlation = -0.2281) by strain gauge and the sampling moiré method and their derivatives for Zone 1 using 2 mm grating. (a) Force–strain, (b) average of strain gauge and measured strain, (c) number of frames and strains, (d) position of Zone 1 of the beam.

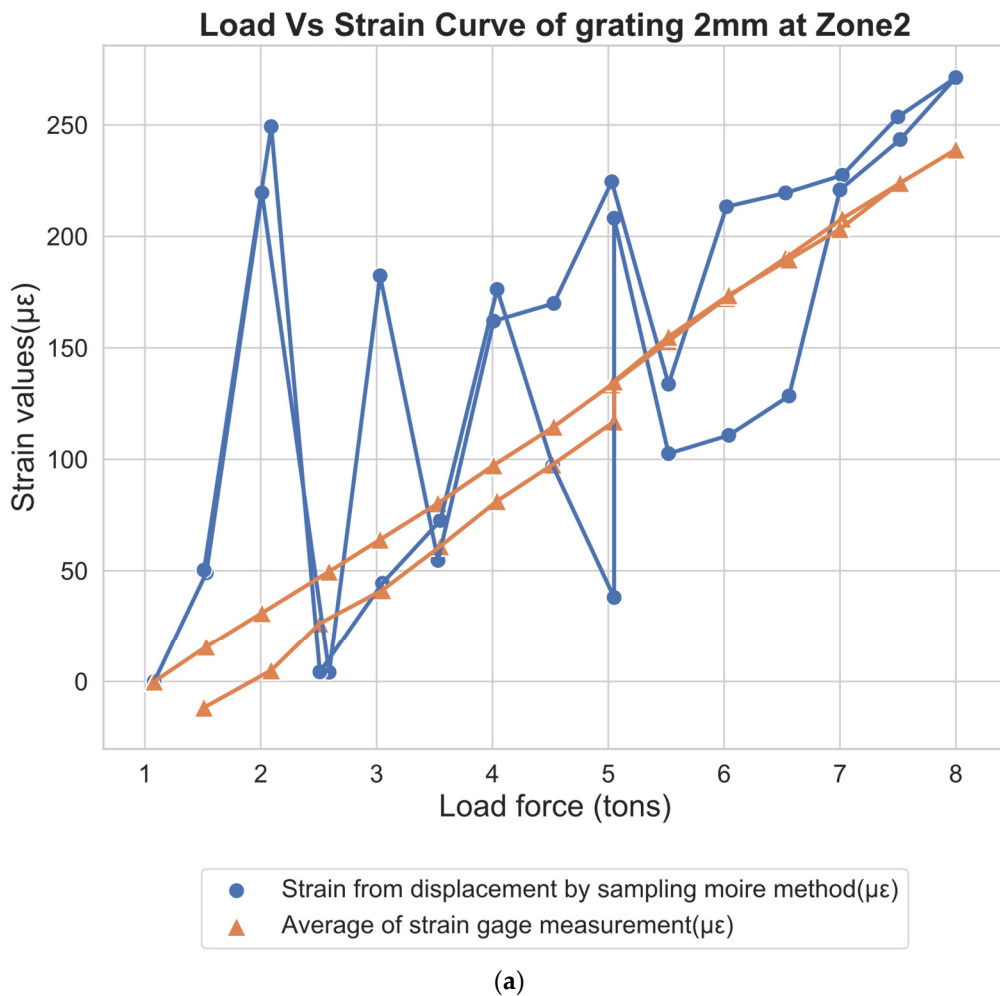


Figure 18. Cont.

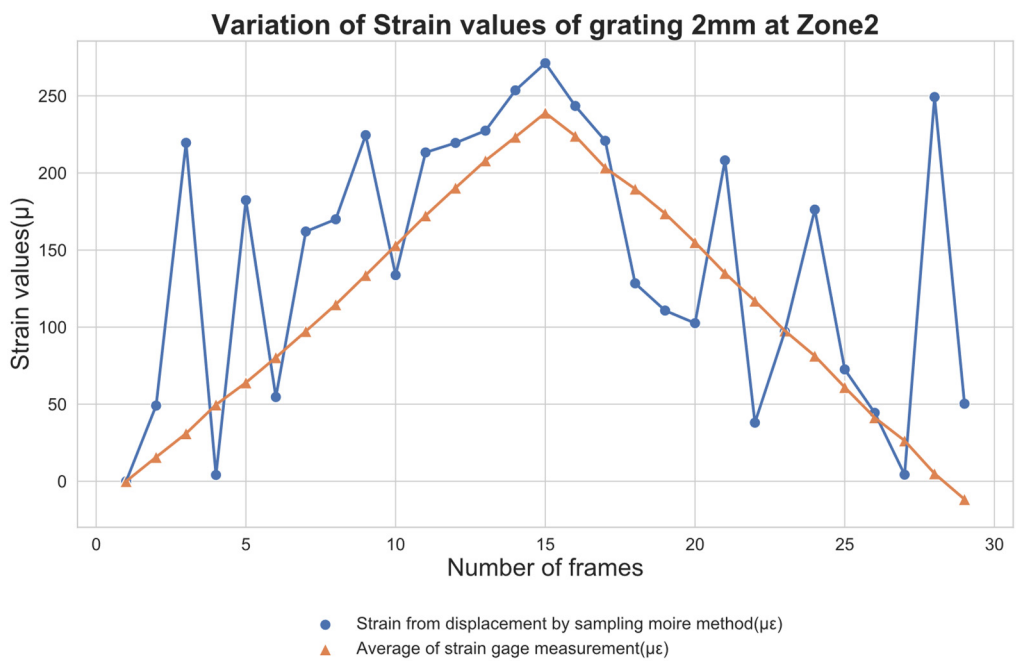
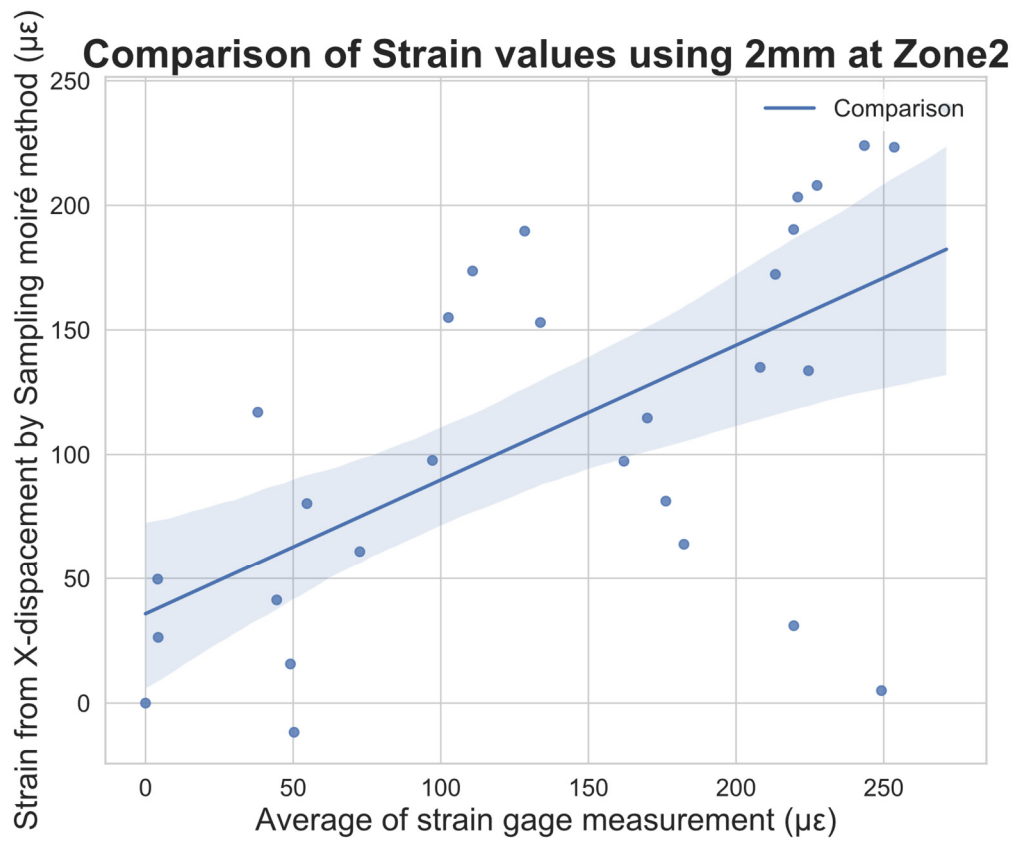


Figure 18. Cont.

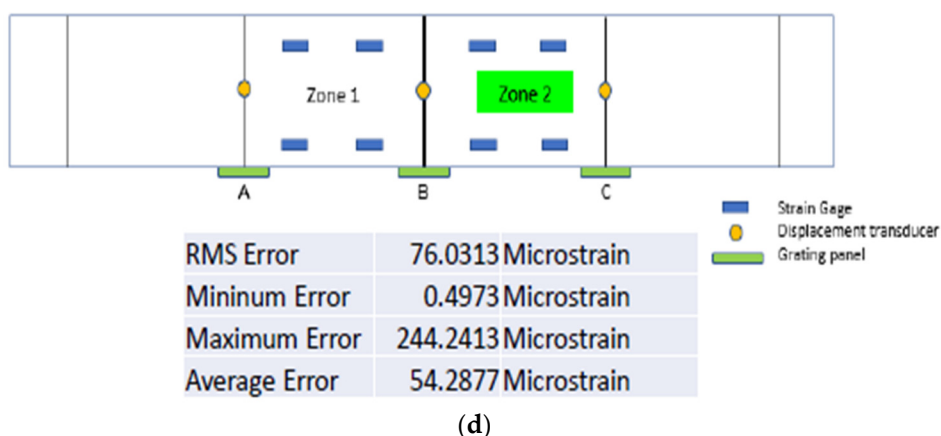


Figure 18. Various graph plots for strain values (coefficient correlation = -0.6157) by strain gauge and the sampling moiré method and their derivatives for Zone 2 using 2 mm grating. (a) Force–strain, (b) average of strain gauge and measured strain, (c) number of frames and strains, (d) position of Zone 2 of the beam.

4. Comprehensive Summary

In the specimen experiment, a 4 mm grating pitch yielded better results for both the y-displacements and strain values calculated. The average resolution was found to be $50\ \mu$ for a 4 mm grating pitch and $40\ \mu$ for a 2 mm grating pitch on the liberal side. Observation revealed that the resolution of the displacement transducer along with the data logger fluctuates by $10\ \mu$ in unloaded conditions and up to $40\ \mu$ when the sensor is loaded for a certain time. Considering the setup that was not devoid of a number of factors that could affect the calculations, the displacement measurement is satisfactory for laboratory conditions.

As far as strain measurement is concerned, Zone 2 has captured the progression of strain to some extent. It has demonstrated that strain measurement is possible by the moiré measurement scheme with improvement in resolution.

5. Discussions

The sampling moiré method originally proposed by Morimoto and Fujigaki (2009) was assessed for displacement measurement through a series of tests conducted using the CMOS sensor to establish the efficacy of the method. Further, the same tests were conducted with a CCTV camera to examine if the results were reproducible. Finally, an experiment was conducted on the specimen by loading to obtain displacements in both directions and calculate strain from x-displacement.

We can conclude that this method is a promising visual displacement measurement technique for the Structural Engineering Laboratory using CCTV cameras. It displays adequate performance unaffected by the input voltage and temperature changes, unlike other traditional sensors. Low-cost, low-resolution CCTV cameras have adequate resolution to perform consistently, which is preferable. Strain measurement is also viable from this measurement scheme, as is evident from the above results, with improvements.

There are some inherent constraints in the moiré scheme that have to do with both the grating and the camera. In the case of the grating, the quality of printing is critical. Even with the 300 dpi digital printing technique, the best that could be procured, there exist inconsistencies in the printing, which is evident when the camera is close to the specimen. Similarly, a CCTV camera has a limited usable area coverage for analysis due to its wide-angle lens. In this case, only a circular area at the center, with a radius of $1/4$ th of the width of a frame, is at disposal. Likewise, for the short gauge length issue, the displacement resolution of $55\ \mu$ from the available measurement scheme to achieve a $7\ \mu$ resolution as calculated above for strain measurement from the current setup is indeed

challenging. For this, an immense improvement of about seven times the current resolution is required.

The recommendations for further improvement of the scheme would be to resolve the issue of the printing quality of the grating pattern optimized over the resolution sought. Moreover, exploring the strain measurement by the scheme by improving the resolution, adjusting the gauge length, etc. Furthermore, upgrading the physical video retrieval system as of now to real-time displacement measurement could be a prominent scope for laboratory platforms.

Author Contributions: Conceptualization, R.T. and P.T.; methodology, R.T.; software, R.T.; validation, R.T., P.T. and S.E.; formal analysis, R.T.; investigation, R.T.; resources, P.T.; data curation, R.T.; writing—original draft preparation, R.T.; writing—review and editing, S.E.; visualization, P.T.; supervision, P.T. and S.E.; project administration, P.T. All authors have read and agreed to the published version of the manuscript.

Funding: This research received no external funding.

Conflicts of Interest: The authors declare no conflict of interest.

References

1. Yan, X.; Brownjohn, J.M.W. Vision-based systems for structural deformation measurement: Case studies. *Proc. Inst. Civ. Eng.-Struct. Build.* **2018**, *171*, 917–930. [[CrossRef](#)]
2. Morimoto, Y.; Fujigaki, M. Theory and Application of Sampling Moiré. In *Recent Advances in Mechanics*; Springer: Berlin/Heidelberg, Germany, 2011; pp. 227–248.
3. Morimoto, Y.; Fujigaki, M. Accuracy of sampling moiré method. In Proceedings of the International Society for Optical Engineering, 2008, Nanjing, China, 25 August 2009; Volume 7375, pp. 2–7. [[CrossRef](#)]
4. Ri, S.; Fujigaki, M.; Morimoto, Y. Sampling Moiré Method for Accurate Small Deformation Distribution Measurement. *Exp. Mech.* **2010**, *50*, 501–508. [[CrossRef](#)]
5. Ri, S.; Muramatsu, T. Theoretical error analysis of the sampling moiré method and phase compensation methodology for single-shot phase analysis. *Appl. Opt.* **2012**, *51*, 3214–3223. [[CrossRef](#)] [[PubMed](#)]
6. Ri, S.; Muramatsu, T.; Saka, M. A Phase Compensation Technique of Sampling Moiré Method for Accurate Single-Shot Phase Analysis. *Appl. Mech. Mater.* **2011**, *70*, 243–248. [[CrossRef](#)]
7. Ri, S.; Muramatsu, T.; Saka, M.; Nanbara, K.; Kobayashi, D. Accuracy of the Sampling Moiré Method and its Application to Deflection Measurements of Large-Scale Structures. *Exp. Mech.* **2012**, *52*, 331–340. [[CrossRef](#)]
8. Nakabo, M.; Fujigaki, M.; Morimoto, Y.; Sasatani, Y.; Kondo, H.; Hara, T. Development of Sampling Moiré Camera for Landslide Prediction by Small Displacement Measurement. In *Conference Proceedings of the Society for Experimental Mechanics Series*; Springer: Berlin/Heidelberg, Germany, 2011; Volume 5, pp. 323–330. [[CrossRef](#)]
9. Morimoto, Y.; Fujigaki, M.; Masaya, A.; Shimo, K.; Hanada, R.; Seto, H. Shape and strain measurement of rotating tire by sampling moiré method. *SAE Int. J. Mater. Manuf.* **2011**, *4*, 1107–1113. [[CrossRef](#)]
10. Hanada, R.; Miyazawa, M.; Fujigaki, M.; Simo, K.; Morimoto, Y. A sampling moiré method to measure the dynamic shape and strain of rotating tires. *Tire Sci. Technol.* **2013**, *41*, 214–225. [[CrossRef](#)]
11. Ri, S.; Wang, Q.; Tsuda, H.; Shirasaki, H.; Kuribayashi, K. Displacement measurement of concrete bridges by the sampling Moiré method based on phase analysis of repeated pattern. *Strain* **2020**, *56*, e12351. [[CrossRef](#)]
12. Ri, S.; Tsuda, H.; Chang, K.; Hsu, S.; Lo, F.; Lee, T. Dynamic deformation measurement by the sampling Moiré method from video recording and its application to bridge engineering. *Exp. Tech.* **2020**, *44*, 313–327. [[CrossRef](#)]
13. Ri, S.; Muramatsu, T. A simple technique for measuring thickness distribution of transparent plates from a single image by using the sampling moiré method. *Meas. Sci. Technol.* **2010**, *21*, 025305. [[CrossRef](#)]
14. Fujigaki, M.; Sasatani, Y.; Masaya, A.; Kondo, H.; Nakabo, M.; Hara, T.; Kurokawa, N. Development of Sampling Moiré Camera for Real-Time Phase Analysis. *Appl. Mech. Mater.* **2011**, *83*, 48–53. [[CrossRef](#)]
15. Ri, S.; Numayama, T.; Saka, M.; Nanbara, K.; Kobayashi, D. Noncontact Deflection Distribution Measurement for Large-Scale Structures by Advanced Image Processing Technique. *Mater. Trans.* **2012**, *53*, 323–329. [[CrossRef](#)]
16. Chen, C.F.; Mao, F.S.; Yu, J.Y. A digital image correlation-aided sampling moiré method for high-accurate in-plane displacement measurements. *Measurement* **2021**, *182*, 109699. [[CrossRef](#)]
17. Shiri, R.; Najafi, A.; Habibi, M. Sampling moiré technique and the dynamics of a spreading droplet on a solid surface. *Meas. Sci. Technol.* **2014**, *25*, 035305. [[CrossRef](#)]
18. Ri, S.; Fujigaki, M.; Matui, T.; Morimoto, Y. Deformation Measurement by Phase-shifted Sampling Moiré Method. In Proceedings of the XIth International Congress and Exposition, 2008 SEM Conference, Orlando, FL, USA, 2–5 June 2008; pp. 1–7.

19. Shimo, K.; Fujigaki, M.; Masaya, A.; Morimoto, Y. Development of dynamic shape and strain measurement system by sampling moire method. In Proceedings of the Fourth International Conference on Experimental Mechanics, Singapore, 14 April 2010; Volume 7522, pp. 1308–1316.
20. Fujigaki, M.; Shimo, K.; Masaya, A.; Morimoto, Y. Dynamic shape and strain measurements of rotating tire using a sampling moiré method. *Opt. Eng.* **2011**, *50*, 101506. [[CrossRef](#)]
21. Hara, T.; Nakabo, M.; Fujigaki, M. Dynamic deformation measurement of real bridge using sampling moiré camera. In Proceedings of the 2013 IEEE Conference Anthology, Anthology, China, 1–8 January 2013. [[CrossRef](#)]
22. Lydon, D.; Lydon, M.; Kromanis, R.; Dong, C.Z.; Catbas, N.; Taylor, S. Bridge damage detection approach using a roving camera technique. *Sensors* **2021**, *21*, 1246. [[CrossRef](#)] [[PubMed](#)]
23. Sakiyama, F.I.H.; Lehmann, F.; Garrecht, H. A novel runtime algorithm for the real-time analysis and detection of unexpected changes in a real-size SHM network with quasi-distributed FBG sensors. *Sensors* **2021**, *21*, 2871. [[CrossRef](#)]
24. Kromanis, R. Characterizing Footbridge Response from Cyclist Crossings with Computer Vision-Based Monitoring. In *International Workshop on Civil Structural Health Monitoring*; Springer: Cham, Switzerland, 2021; pp. 83–95.
25. Kromanis, R.; Kripakaran, P. A multiple camera position approach for accurate displacement measurement using computer vision. *J. Civ. Struct. Health Monit.* **2021**, *11*, 661–678. [[CrossRef](#)]
26. Voordijk, H.; Kromanis, R. Technological mediation and civil structure condition assessment: The case of vision-based systems. *Civ. Eng. Environ. Syst.* **2022**, *39*, 48–65. [[CrossRef](#)]
27. Kromanis, R.; Kripakaran, P. Predicting thermal response of bridges using regression models derived from measurement histories. *Comput. Struct.* **2014**, *136*, 64–77. [[CrossRef](#)]
28. Kromanis, R.; Elias, S. Measuring Dynamic Response of the Wilford Suspension Bridge with a Vision-Based Measurement System: A Case Study. In *European Workshop on Structural Health Monitoring*; Springer: Cham, Switzerland, 2023; pp. 280–289.
29. Sakiyama, F.I.; Veríssimo, G.S.; Lehmann, F.; Garrecht, H. Quantifying the extent of local damage of a 60-year-old prestressed concrete bridge: A hybrid SHM approach. *Struct. Health Monit.* **2022**. [[CrossRef](#)]